UNIVERSITY POLITEHNICA OF BUCHAREST

DOCTORAL SCHOOL OF ELECTRICAL ENGINEERING

SUMMARY

DOCTORAL THESIS

CONTRIBUTIONS TO THE STUDY OF THE CELL MEMBRANES PERMEABILIZATION BY EXPOSURE TO ELECTRIC FIELD

Author: Eng. Ana-Maria SANDU

Doctoral supervisor: Prof. Dr. Eng. Mihaela MOREGA

Bucharest, 2022

CONTENT OF THESIS

INTRODUCTION

The present paper entitled "Contributions to the study of the cell membranes permeabilization by exposure to electric field" is structured in three parts and aims to combine the elements of optical microscopy and numerical simulation.

The first part of the thesis presents an analysis of the specialized literature in which are presented the general elements of the electroporation phenomenon and its applications, from where I noticed that the subject is intensely studied by researchers. Following the research, I found an increase in the interest in numerical modeling of the electroporation phenomenon, which can lead to the efficiency of the technologies applied in various bio-medical interventions. Thus, over time, numerical models have been created starting from single spherical cells to the modeling of realistic cells, or of multiple cellular structures obtained from optical microscopy. Starting from these observations, the second part describes the optical methods that I decided to use to obtain realistic cellular structures implemented in the last part of the paper.

Therefore, the third part presents several studies performed by numerical modeling starting from their validation by comparison with the existing analytical model in the literature, up to realistic cellular structures to see how certain parameters (membrane thickness, the shape of the cells, the frequency, the distance between the cells, etc.) influence their behavior in electric field. The conclusions of each study are presented in the last chapter along with the original contributions and perspectives for further development.

CHAPTER 1
GENERAL ELEMENTS OF CELL ELECTROPHYSIOLOGY

Electropermeabilization is the general process of increasing the permeability of cell membranes to various substances, facilitating their transition between the indoor and outdoor cell environment, by exposure to a variable electric field. The process is highly dependent, both on the characteristics of the electric field (amplitude, waveform, frequency, and spatial distribution), and on the electrical and morphological properties of the cells.

Current research in this field approaches both experimental and computational analysis in a complementary way. Numerical simulations, taking into account realistic cell shapes and field exposure conditions, can complement experimental investigations by opening perspectives and providing quantitative data. Over time, simplified models, corresponding to different biological components, from bacteria and cells to tissues, have been investigated by numerical simulation and analysis. Their behavior during exposure to an electric field was analyzed for various purposes: determining the optimal electric field conditions, such as threshold values for triggering electropermeabilization, quantifying the electrical properties of the membrane, and intracellular and extracellular media.

Stages of electropermeabilization [10]:

- *Initiation*: electrical conductivity and permeability begin to increase when the transmembrane voltage exceeds a critical value. The duration times for this stage are nanoseconds for electrical conductivity and microseconds for permeability;
- *Expansion*: occurs as long as the transmembrane voltage remains at the critical value, and the electrical conductivity of the membrane and permeability persist and/or intensify until the end of the pulse (milliseconds);
- *Partial recovery*: after the transmembrane voltage drops below the critical value, the conductivity and permeability of the membrane decrease rapidly, but not completely, stabilizing at a level that still allows transmembrane diffusion of ions and molecules. The duration times of this stage are microseconds for conductivity and milliseconds for permeability;

- *Resealing*: at this stage the membrane gradually recovers its physiological level of impermeability (unless the damage was irreversible and the cell loses viability), lasting from seconds to minutes for temperatures of 20-37 ° C, or hours at temperatures of 4 ° C.
- *Memory*: even after full membrane resealing, the cell may show changes in its physiological processes and reactions to stressors before its final return to its normal state.

Fig. 1.1 suggestively illustrates the steps of forming transmembrane pores, under the action of the applied electric field from outside the membrane and respectively of sealing the pores when suppressing the applied field.

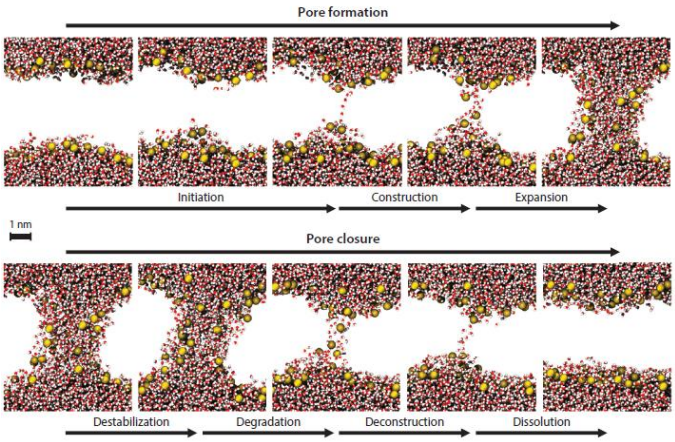

Fig. 1.1 The life cycle of an electrically induced pore in the lipid bilayer of the membrane. The stages of pore formation and sealing are displayed in the order in which they occur. Formation begins with the onset of the electric field, and sealing begins with the cessation of the field. Image is taken from [10].

CHAPTER 2
EXPERIMENTAL ASPECTS OF ELECTROPERMEABILIZATION

Electropermeabilization of the cell membrane is performed with the help of special laboratory equipment called electroporators, which allow the evaluation of several samples simultaneously on microscopy preparations with the same sets of special electrodes for cell cultures. Electroporators can be set for different operating parameters, allowing researchers to optimize the power of the electric field depending on the type of cell and the presence or absence of the cell wall.
An electroporator consists of a high voltage power supply, a pulse generator, a control unit, a user interface, and an output module (Fig. 2.1).

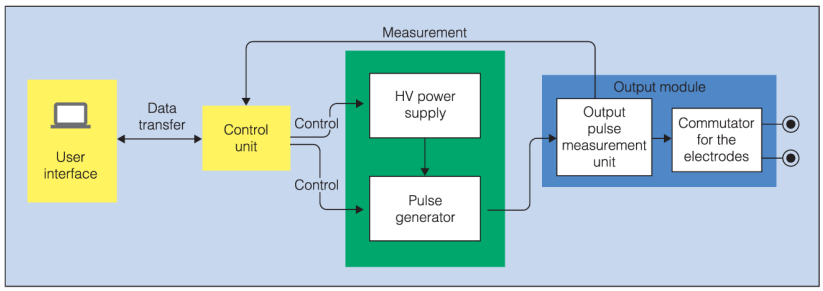

Fig. 2.1 Block diagram of an electroporator. Image is taken from [32]

The user interface allows you to set the pulse parameters, depending on the desired application. It is necessary for the device to measure the parameters of the supplied pulses and to warn the user in case of malfunction. A high voltage power supply and a pulse generator are required to generate and model

electrical pulses. The output module includes the output pulse measurement unit and a switch for high voltage pulses on different electrodes (if more than one electrode is used).

Electroporators are classified according to the field and the applications for which they are used as follows: clinical, industrial, and laboratory.

The main applications of electroporation are in medicine (electrochemotherapy, gene electrotransfer, biomolecule extraction, cell fusion), but also in food biotechnology, many directions are developing (inactivation of microbes or other microorganisms, biomass drying, biomolecule extraction, microfluidic applications).

As each type of application involves the use of other cell types, a deep knowledge of the working conditions and general characteristics of the behavior of lipid membranes in a time-varying electric field is required [48], [49]:

• the physical characteristics of the cells (dimensions, circular or elongated shapes, positioning concerning the orientation of the applied electric field, physical properties of the material: permittivities, electrical conductivities);

• parameters of the applied external electric field (electric field strength, waveform, frequency, signal application time) and application mode (with needle electrodes, of other shapes, or in the uniform electric field created in a flat capacitor type device);

• environmental conditions (temperature, pH, and if they are cell cultures, the electrical properties of the extracellular environment are also important).

For the material properties, important are: 1) the electrical permittivities of the membrane, cytoplasm, and extracellular environment, and 2) the electrical conductivities of the same three subdomains. As with all biological environments, the electrical properties vary significantly depending on the frequency of the applied electric field, especially on certain subdomains of the Hertzian wave spectrum.

In Fig. 2.2 is the simplified schematic representation of a two-layer spherical cell, representing its components and the association of material properties (conductivity and electrical permittivity, σ and ε) for each: cytoplasm (σ_c, ε_c), membrane (σ_m, ε_m)) and the extracellular environment (σ_e, ε_e). Starting from this idealized representation, but including the significant properties that are important in the development of the electropermeabilization phenomenon, several numerical simulation models were made modifying the electrical and morphological properties of the spherical cell to observe their influence on the induced transmembrane voltage (ITV).

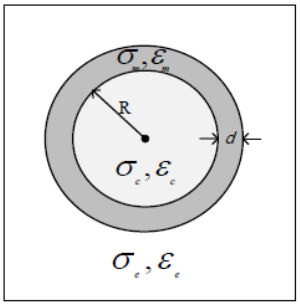

Fig. 2.2 Two-layer spherical cell model, σ and ε represent the electrical conductivity, respectively the electrical permittivity for each subdomain

CHAPTER 3
EVALUATION OF BIOLOGICAL SAMPLES BY OPTICAL MICROSCOPY TO ANALYSE THE EFFECTS OF ELECTROPERMEABILIZATION

Interference and dark-field optical microscopy techniques have the advantage that they can be used for the study of biological samples in different environments, without the need for special

preparations and without damaging the samples. In addition, they provide some important information that is not available through other techniques.

Classical light microscopy uses staining chemicals to study biological samples in the bright field. These chromatographic markers help to differentiate certain areas of tissue or cells, but at the same time require complex protocols, time, and money to prepare and can change the composition of the sample. These techniques determine the values of the dimensions (2D), in a transverse plane on the direction of light propagation, and the staining mode provides information about the categories of different cells.
That is why, in recent years, analysis techniques have been sought to provide information about biological samples without the need for staining markers. In this context is the holographic microscopy technique which is dedicated to the study of samples in their natural environment and which provides quantitative information both in the transverse plane and in the direction of light propagation, resulting in 3D images. Another technique that provides 3D imaging of biological samples is dark field microscopy which uses scanning along the direction of propagation at 100 nm pitch. This, combined with the technique of hyperspectral microscopy, provides multiple information about biological samples.

Were studied these two techniques and used them in the acquisition of images of different types of cells in cultures to use them for further processing and to extract information by calculating specific parameters. Holographic microscopy, with the advantage of real-time acquisition, was used to record cells during and after the application of the electroporation pulse, providing thousands of frames that were processed to highlight the effects of electroporation. The images recorded using dark-field microscopy, I will use in the future as input in numerical simulations because this type of microscope offers a high resolution on the 3 axes, and the cellular compartments (cytoplasm, nucleus) are well highlighted.

To obtain images of realistic cells compatible with the numerical computing environment, it was necessary to process the phase images obtained by digital holographic microscopy by following the steps: a) segmentation using Matlab software; b) cell shape boundaries selection in AutoCAD software for contouring and delimiting different membrane thicknesses; c) graphical conversion of the file to ensure compatibility with the numerical computing environment; d) choosing the appropriate discretization network for the three compartments (outside / inside the cell and cell membrane).

Fig. 3.1 illustrates an example of an experimentally recorded hologram, and Fig. 3.2 illustrates the main steps of image processing for two different cells. In the first step, an adaptive binary filter was used to segment the phase image. Then, dilatation and erosion transformations were applied to the binary image to ensure the compactness of the selected contour. The result of these operations was a mask, which applied to the initial phase image generated an image from which the area of interest was selected. This image was then imported into AutoCAD software, where the cell contour was manually selected. The membrane was made by duplicating the contour and rescaling to ensure different thicknesses using the offset command. The cell model obtained at the end after applying all the steps was saved in a format compatible with Comsol Multiphysics.

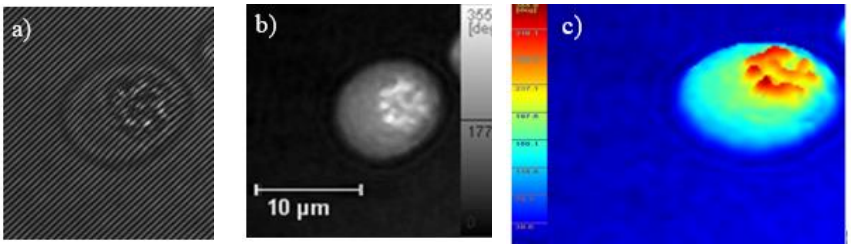

Fig. 3.1a) Experimental recorded hologram, b) Reconstructed phase image; c) 3D representation [23]

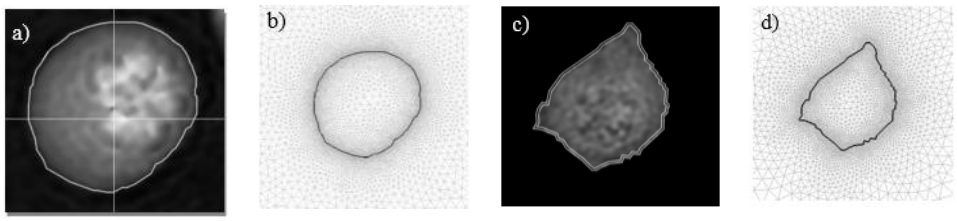

Fig. 3.2 Image processing steps for CELL_A (left) and CELL_B (right): a) and c) PIs resulting from holograms reconstruction after segmentation; b) and d) cells imported in COMSOL with real contours and an adequate mesh used for the numerical model (a crop from the entire domain [23]

A study conducted with images acquired by digital holographic microscopy was aimed at investigating the behavior of cells exposed to bipolar pulses of different amplitudes in experiments for electroporation. 5400 experimental holograms were recorded for each cell for 90 seconds: 100 frames before the pulse were applied and the rest during and after the electroporation pulse was applied. The reconstructions, as phase images, were processed to obtain values of some global parameters: the area occupied by the cell, the dry mass, the entropy, and their variations in time.

To locally characterize the phase difference fluctuations in certain points of interest, we chose to calculate the correlation and autocorrelation functions. This approach by calculating the correlation and autocorrelation functions is a new method from two points of view: their calculation for the study of the local properties of electroporated cells and the application of these functions on phase images.

During the 90 seconds investigated, was observed a decrease in the area occupied by the cell for amplitudes of the electroporation pulse of 0.6 kV and 0.8 kV. In the case of 1 kV pulses, there were large variations in the parameters with many cells swelling and collapsing (Fig. 3.3).

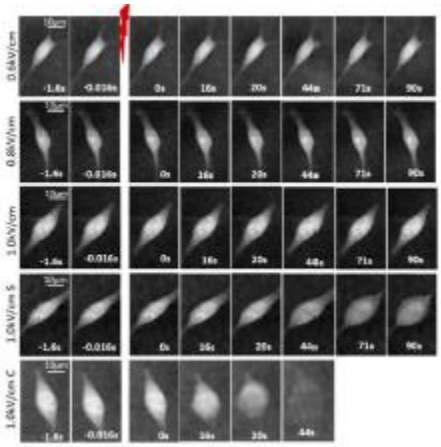

Fig. 3.3 Examples of time series of QPIs of cells electroporated with different pulses amplitudes. The last two rows present cells electroporated with 1 kV/cm pulses showing a specific behavior: one is swelling (S), the other one is collapsing (C). The EP moment is marked with a red arrow and the time moment of the frame is presented on each image. For each category of cells media materials are available: Line 1 (0.6 kV/cm), Line 2 (0.8 kV/cm), Line 3 (1.0 kV/cm), Line 4 (1.0 kV/cm S), and Line 5 (1.0 kV/cm C) [86].

The autocorrelation functions were calculated at three points: the point of maximum phase difference and at two points near the cell membrane, located along a line parallel to the field lines and passing through the point of maximum phase difference. Autocorrelation functions indicate that the central regions of the cell are much less affected by electroporation than those closer to the cell membrane.

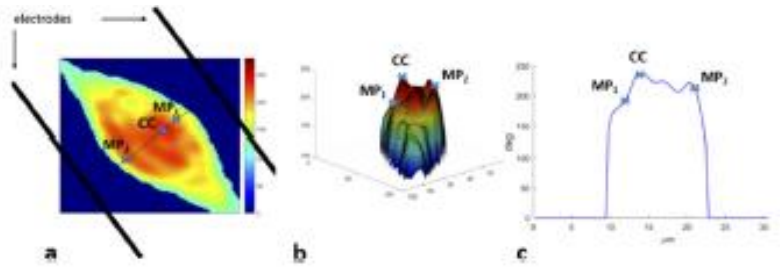

Fig. 3.4 Definition of regions for which the autocorrelation functions were calculated. (a) QPI of a cell: the color scale represents the phase shift values from 0 to 250deg, the two black sticks represent the electrodes, the dashed line shows the electric field direction; (b) 3D image of the same cell; (c) The corresponding phase shift profile along the dashed line. In all three images, the light-blue crosses represent the three regions chosen for the computation of the time-dependent autocorrelation functions: CC – a central point, MP1, and MP2 – midpoints [86]

An application for which I acquired and processed images using dark-field microscopy CytoViva [88] was the study of how cells are distributed in culture on superparamagnetic micromagnets made by direct laser beam writing, by two-photon polymerization of a superparamagnetic composite photopolymerizable, by colleagues from the Institute of Laser, Plasma and Radiation Physics, Măgurele. Control samples and samples introduced in the static magnetic field were studied.

Micromagnets are areas of polymer in which magnetic nanoparticles have been incorporated and have been designed as a 2D microarray similar to a chessboard in which there is an alternation between paramagnetic and non-magnetic areas. Fibroblast cells were cultured on them and then exposed to a static magnetic field of 1.3 T. It was observed that for the samples not exposed to a magnetic field, the incubated fibroblasts were uniformly attached to the entire surface of the 2D microarray, without being influenced by the paramagnetic and non-magnetic areas. While, under the influence of a magnetic field, they settled only in the area of superparamagnetic micromagnets. This method can offer the possibility of manufacturing biocompatible micromagnets with well-defined geometries for optimal integration of skin grafts into tissues.

In Fig. 3.5 are images of the fabricated structures before cells are cultured on them. The distribution of yellow dots is observed only inside the squares in the paramagnetic zones and their absence in the non-magnetic zones.

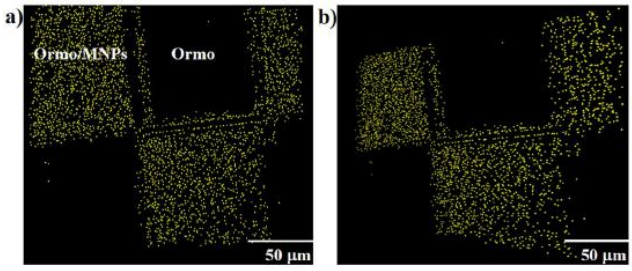

Fig. 3.5 2D representation of the microarray obtained using the 3D module of the CytoViva dark field microscope (yellow dots represent superparamagnetic nanoparticles): a) top view; b) inclined view. Images of structures before cells are cultured [88]

Fig. 3.6 represents the distribution of the cells in culture on the microarray with the paramagnetic and non-magnetic zones. On the top row is the image of a sample introduced into the 1.3T magnetic field, and on the bottom row is a control sample, with cells cultured on the same type of structures, but without being exposed to the magnetic field. The different organization of the cells is observed in the two situations: with the magnetic field or without the magnetic field. In the situation without a magnetic field, the cells are evenly distributed on both types of squares, while in the situation with a magnetic field, they

are distributed only on the paramagnetic areas (these are signaled by the presence of identified yellow dots and fabricated structures).

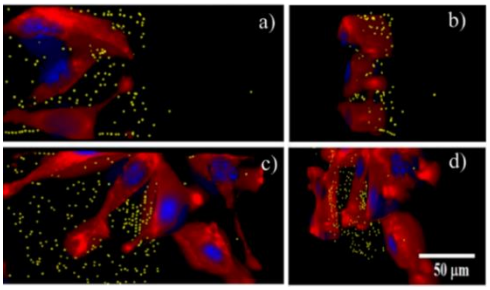

Fig. 3.6 3D representation of microarrays (a, c) top view and (b, d) inclined view of samples with color highlighting of the three components intended for analysis: nuclei (blue), cytoskeleton (red), and superparamagnetic nanoparticles (yellow). In presence (a, b) and absence of static magnetic field (c, d) [88]

CHAPTER 4
ANALYTICAL AND NUMERICAL MODELS OF IDEALIZED CELL STRUCTURES; VALIDATION OF NUMERICAL MODELS

This study consists in the validation of the main characteristics involved in the formulation of numerical models of cell exposure to a uniform electric field, by comparing the results with data from the analytical model from the literature. Very simple numerical models are used (homogeneous and stratified spherical structures), for which there are also analytical solutions.

When a body is exposed to an electric field, its shape and electric properties are essential for determining the distribution of the intensity of the electric field inside and outside it, significant data for the evaluation process of the electroporation phenomenon.

The main advantage of numerical simulation is to obtain quantitative information additional to the simulation by analytical calculation and even experimental results, regarding the behavior and evolution of cells exposed to an electric field. Even though in mathematical simulations it is inherent to adopt simplifying hypotheses (idealizations), models can be used for testing with reduced resources a wide range of characteristics (specific settings for any study), which are difficult to apply to experiments. However, mathematical models must be validated before use in practical applications. In the validation phase, an idealized case of electrical stress was considered, namely the exposure of the spherical body to low-frequency harmonic fields.

For a long time, the most used shapes for the numerical analysis of the electroporation phenomenon were the spherical and ellipsoidal ones, but recently realistic images of cells obtained by optical microscopy began to be used, thus studying the influence of morphological elements on the phenomenon of electroporation. penetration of the electric field into the cellular environment, as well as its impact on the elements of the cellular and subcellular structure. The preferred microscopic methods, in this case, are those that provide 3D information, so obtaining realistic cell shapes and sizes is much more accessible, for example, MHD (digital holographic microscopy) and CytoViva (dark and hyperspectral field microscopy).

The reference used for validation was the analytical model derived by Schwan [97] for the solution of Laplace's equation applied to the electric potential, for spherical layered bodies exposed to uniform steady-state electric field (Fig. 4.1a).

One spherical 3D model (Fig. 4.1b) was first created in COMSOL Multiphysics, as similar to the analytical reference model as possible. Starting from this, two subsequent 2D models were derived: a) a 2D-axial model (Fig. 4.1c) based on axial-symmetry in polar coordinates, which represents the natural reduction of the 3D structure, and b) a 2D-cartesian model (Fig. 4.1d) built as a representation of the

whole cell in Cartesian coordinates which is very useful for the study of realistic cells geometries resulted from microscopy image processing (Fig. 4.1e). Each model was implemented and studied in Comsol AC/DC time-harmonic analysis application mode, at 50 Hz, which is valid for a range of low frequencies up to 10 kHz. In the analytical problem, the space around the spherical body is considered infinitely extended, while for the numerical model the computational field must be limited with artificially boundaries and defined so that the solution of the problem is minimally affected. The configuration and dimensions of the calculation domain are specified for each model, together with the electrical properties of the material (electrical conductivity, σ, and electrical permittivity, ε) (Fig. 4.1). The specific results were then determined and compared against the analytical model, namely: the electric field strengths distributions inside and outside the cell and the ITV along the contour of the membrane. All models produced comparable accurate results and, most important, we could conclude that our 2D - cartesian model, which is particularly useful for further applications based on DHM technique, can represent the behavior of realistic cells in a manner as accurate as of the other models. The accuracy of the results was considered satisfactory, not only based on the comparison with 3D models, but also by the fact that it highlights very well the dielectric demands of interest for electroporation. Both experiments and 3D models show that the highest dielectric stresses (quantified here by the maximum values of ITV) are identified in the regions where the vector **E** (electric field strength) is normally oriented on the membrane surface. The 2D - cartesian model results by applying plane-parallel symmetry, to reduce the computational range to a longitudinal plane (section plane through the cell and enclosure along the electric field lines), in which the identification of maximum dielectric loads is perfectly possible.
The same configuration is extracted from the microscopy images, used to create realistic numerical models - a 2D field in which the flattened cell is in a uniform electric field, oriented parallel to the respective plane (Fig. 4.1e).

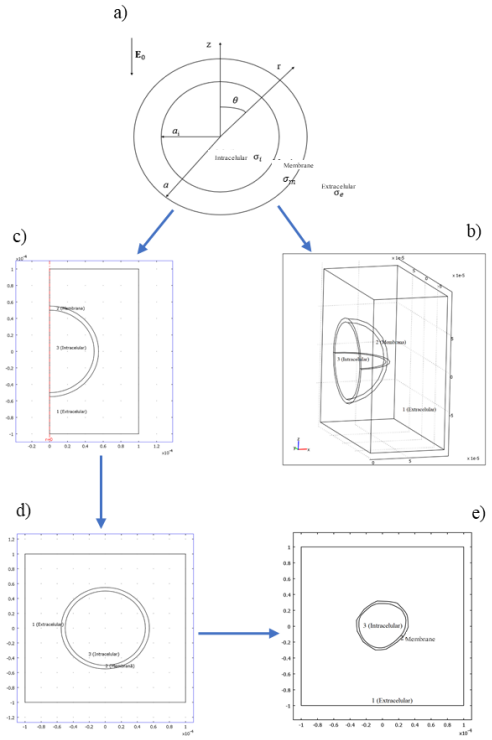

Fig. 4.1 The configuration and dimensions of the calculation domain for each model: a) the inhomogeneous analytical model; b) the 3D spherical model; c) the 2D - axial model; d) the 2D - cartesian model; e) the 2D model of a realistic cell

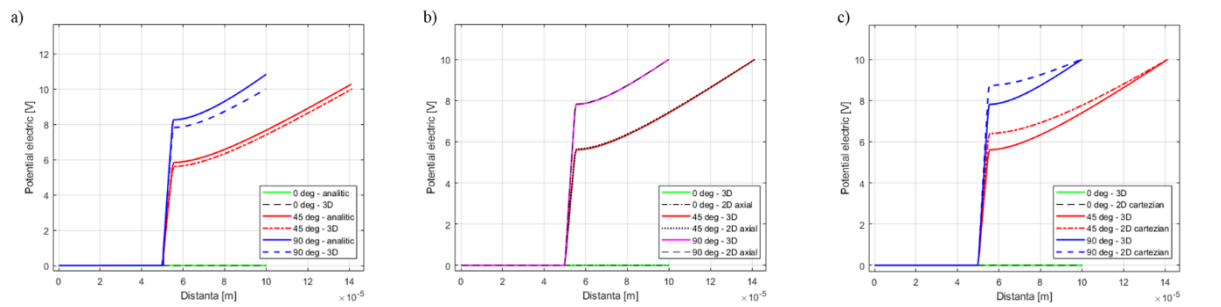

Fig. 4.2 Comparison between the analytical model and the numerical models by graphical representation of the electrical potential at 0°, 45°, 90° degrees: a) the inhomogeneous analytical model and the 3D spherical model; b) 3D spherical model and 2D - axial model; c) 3D spherical model and 2D - cartesian model

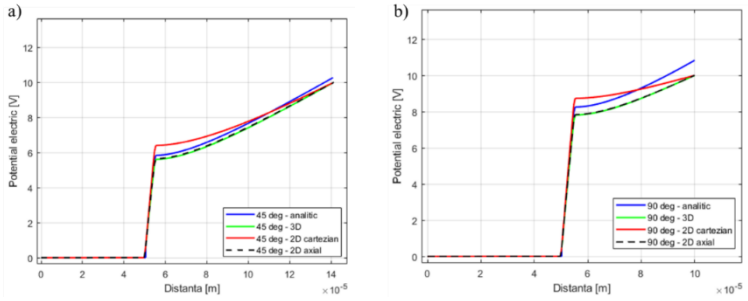

Fig. 4.3 Comparison between the analytical model and the numerical models by the graphical representation of the electrical potential for: a) 45° degree; b) 90° degree

In Fig. 4.2 and Fig.4.3 are the graphical representations of the electrical potential for different angles θ (the angle measured according to the horizontal axis), corresponding to the spherical coordinates based on which the validation of the numerical models was made by comparison with the analytical model from the literature.

During the validation process, also could be verified other principles derived from the simulation studies presented in the literature on the behavior of cells exposed to a uniform electric field, such as the theory that at low frequencies, up to 10 kHz, the membrane is a very good electrical insulating material (its conductivity is of the order of 10-7 S/m), and the induced transmembrane voltage does not depend on the thickness of the membrane.

CHAPTER 5
NUMERICAL MODELS OF REALISTIC CELL STRUCTURES - EXPOSURE TO HARMONIC ELECTRIC FIELD

5.1 DESCRIPTION OF THE NUMERICAL MODEL FOR REALISTIC CELL STRUCTURES AT VARIABLE FREQUENCY

The numerical problem has been formulated similarly to the one used for the idealized circular-shaped cells, described in chapter 4. The computational domain was limited to a rectangular box with dimensions 50 x 50 microns, providing that the applied electric field is uniform close to the boundaries. Then, a uniform electric field with the amplitude of 1 kV/cm was set inside the enclosure. The following dielectric properties were considered for the cellular components: for the membrane, the conductivity was set to $\sigma_m = 3 \cdot 10^{-7}$ S/m and the dielectric constant to $\varepsilon_m = 5$, for the cytoplasm the properties were set to $\sigma_i =$

0.3 S/m și ε_i= 72.5. For the conductive extracellular fluid, the conductivity was set to σ_e= 0.3 S/m and the dielectric constant ε_e=72.5, as shown in literature for low frequencies [100].

Studies of the behavior of the cell in the harmonic electric field at various frequencies, the electrical properties of the material, which are themselves variable with frequency, are expressed using the model proposed by Debye for complex electrical conductivity and complex electrical permittivity, using the frequency as the argument. The Debye model (refers to a single dispersion, valid for a subdomain of frequencies) proposes the expressions in the complex, according to [99], where the coefficients are made explicit in Fig. 5.1. The permittivities ε_s and ε_∞ occur as relative values (dielectric constants), and $\varepsilon_o = 8.854 \cdot 10^{-12}$ [F/m] is the electrical permittivity of the vacuum:

$$\underline{\sigma}(f) = \sigma_\infty + \frac{\sigma_s - \sigma_\infty}{1 + j(f/f_c)} + 2\pi f \varepsilon_\infty \varepsilon_o \tag{5.1}$$

$$\underline{\varepsilon}_r(f) = \frac{\sigma_s}{j\omega\varepsilon_o} + \frac{\varepsilon_s - \varepsilon_\infty}{1 + j\,(f/f_c)} + \varepsilon_\infty \tag{5.2}$$

$$\sigma(f) = \sigma_s + \frac{\omega\varepsilon_o(\varepsilon_s - \varepsilon_\infty)}{1 + (f/f_c)^2}(f/f_c) \tag{5.3}$$

$$\varepsilon_r(f) = \varepsilon_\infty + \frac{\varepsilon_s - \varepsilon_\infty}{1 + (f/f_c)^2} \tag{5.4}$$

The Debye model provides expressions for the frequency functions of the two material properties (electrical conductivity and dielectric constant) for the membrane and the cytoplasmic aqueous media; this study considers the extracellular environment with electrical properties similar to the cytoplasm [22].

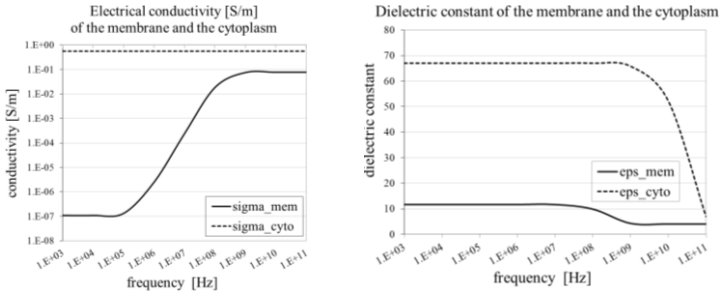

Fig. 5.1 Frequency-dependent dielectric properties of cell components (Debye models) [24] (the vertical axis is valid for both quantities; values are in [S/m] for conductivity and dimensionless for dielectric constant and the scales are logarithmic).

In Fig. 5.1 these functions are represented graphically, on a logarithmic scale, for each cellular component, throughout the spectrum of frequencies that are of interest in electroporation experiments. It is visible that the dispersion of the electrical conductivity of the membrane has three major intervals, which match the subdivisions of the frequency spectrum to electroporation (low-frequency LF, medium frequency MF, and high-frequency HF), while the dispersion of the dielectric constant of the membrane is limited at the common range LF + MF and the range HF. Dispersions of the cytoplasm and the electrical properties of the extracellular environment occur at very high frequencies and to a small extent influence the electroporation process. In Fig. 5.2 are the representations for the realistic cells used in the studies analyzed in this chapter, from where the differences in size and shape can be observed since they are not on the same scale.

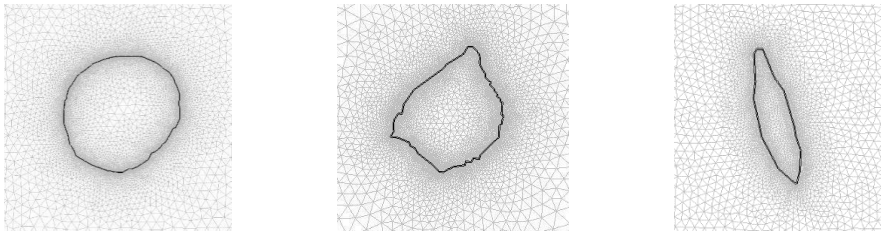

Fig. 5.2 Cells imported in COMSOL with real contours and an adequate mesh used for the numerical model

5.2 STUDY OF THE INFLUENCE OF MEMBRANE THICKNESS ON THE INDUCED TRANSMEMBRANE VOLTAGE (ITV) AT LOW FREQUENCY

The study aims to perform a quantitative analysis of the influence that membrane thickness can have on the accuracy with which important indicators are determined in assessing the threshold for triggering electroporation (in particular ITV values). Assessing the uncertainties generated by small variations in membrane thickness, as an important date of the problem, is useful in the future development of cellular models. The normal thickness of the membrane is approx. three orders of magnitude smaller than the radius of a spheroidal cell (for example 5 nm versus 5 μm). The membrane is therefore a computational subdomain of the type of a very thin layer of material, with very different electrical properties from those of the environment. For the accuracy of the model, the natural solution is to represent the membrane at its realistic thickness, while for the economic management of computing resources there is either a tendency to oversize the thickness or to replace this thin layer with a crossing surface (border) where to be specified suitable conditions for electrical quantities. In model formulation, these trends lead to different numerical implementations, which can generate solutions with different values. Uncertainty management is the main goal pursued here. The tests below assess the possible errors caused by oversizing the thickness of the membrane.

2D - Cartesian models were used:

* Realistic cell_A and Realistic cell_B - two optically analyzed cells obtained by reconstruction based on microscopic images (procedure described in Chapter 3) resulted in computational domains;
* Circular cell_A and Circular cell_B are their correspondents in circular shapes, equivalent based on the equality of the area visible in the microscope image, having the radial dimensions of 5.28 μm and 2.9 μm respectively.

For all 4 cells with different morphologies, a test was performed to analyze the response to low-frequency electrical stress, by determining the variation of ITV values on the circumference, at various membrane thicknesses, in the range of 5 nm ... 100 nm. The applied electric field strength has the value of 1 kV / cm, and the electrical properties of the cellular components are according to [100].

Fig. 5.3 and Fig. 5.4 represent the induced transmembrane voltage for different membrane thicknesses between 5 nm and 100 nm, of realistic cells compared to the corresponding spherical cells. In this case, it can be seen that the thickness of the membrane does not influence the membrane voltage induced by exposure to the uniform electric field, with harmonic variation over time, at low frequencies. In the case of realistic cells, due to the irregular shape of the contour, very small, negligible differences may occur in cases of increasing the thickness of the membrane in a narrow range (up to about 100 nm). Even with these circular deviations, the sinusoidal (or cosinusoidal) profile of the ITV distribution on the cell circumference largely maintains its appearance from the corresponding circular cells. It is, of course, expected that this profile will become more and more deformed as the shape of the analyzed cell deviates more from the circular shape. The difference in ITV values between B and A configuration cells is due to significant differences in size - type A cells have an area of approx. four times larger than type B cells.
Given these observations, was concluded that even larger membrane thicknesses can be used, with benefits in the balanced density of the discretization network throughout the computing field, with effects

in shortening the processing time of numerical simulations, reducing computing resources, as well as cost reduction.

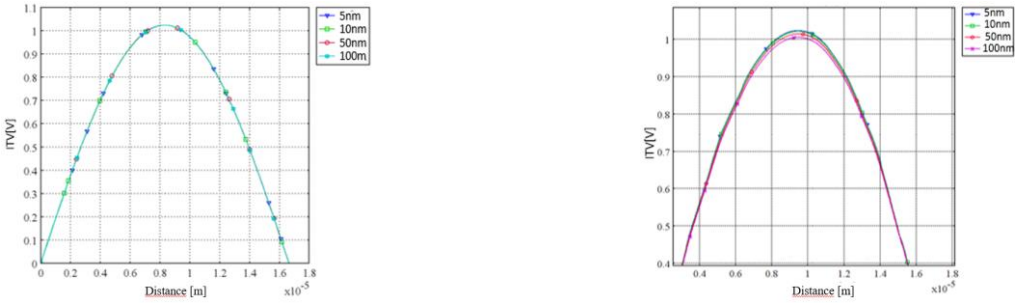

Fig. 5.3 ITV amplitude (absolute value) on half of the cell contour for various membrane thicknesses within the range of 5 to 100nm for a) Circular cell_A and b) Realistic cell_A exposed to a low-frequency electric field [23]

Fig. 5.4 ITV amplitude (absolute value) on the half of the cell contour for various membrane thicknesses within the range of 5 to 100nm for a) Circular cell_B and b) Realistic cell_B exposed to a low-frequency electric field [23]

5.3 STUDY OF THE ELECTRIC FIELD DISTRIBUTION AND THE ITV INDICATOR FOR DIFFERENT CELLULAR MODELS AT LOW FREQUENCY

For non-spherical cells, it is recommended that the induced transmembrane voltage be expressed as a function of the arc length along the membrane, and for uniformity, a standardized version of the arc length should be used [107]. By exposing a cell to a uniformly distributed electric field in an enclosure of the type of a flat capacitor, at low-frequency variation frequencies, its uniform distribution is disturbed, as can be seen in Fig. 5.5a). From Fig. 5.5b) it can be observed that due to the low electrical conductivity of the membrane the electric field is concentrated in the membrane areas that cover the cell poles (the electric field vectors come in a normal direction to the membrane surface), having values two orders of magnitude larger than the applied electric field. Fig. 5.5c) highlights the intensity of the electric field inside the membrane for the Realistic Cell_A.

While the membrane acts as a field concentrator, the field distribution is quasi-uniform inside the cell, with an amplitude of about 25 V/m. Compared to the value of 0.1 MV/m of the applied electric field intensity, the result demonstrates the significant shielding effect when the electric field penetrates, achieved by the membrane on the inner cellular area.

The same behavior is observed in the case of Realistic Cell_B, but with larger discontinuities, as shown in Fig. 5.6. Due to its smaller size compared to Realistic Cell_A, the disturbance caused by it is smaller in terms of the general distribution of the electric field, but the induced membrane electric field is more concentrated in areas where the cell surface is less smooth, Fig. 5.6c).

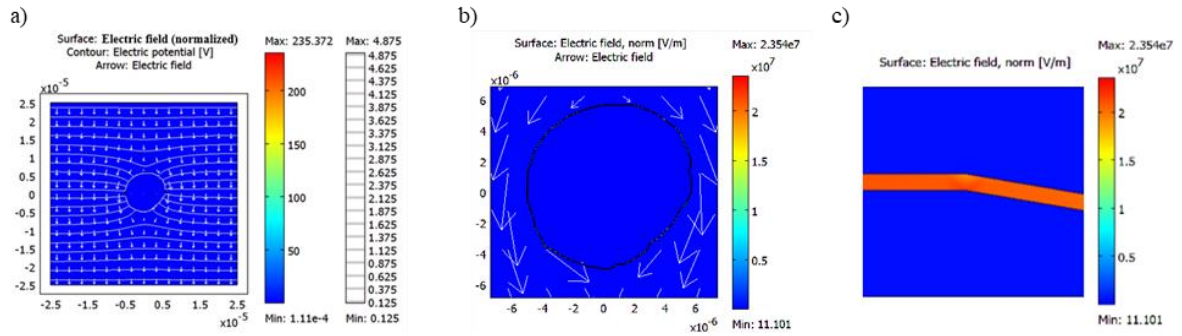

Fig. 5.5 Distribution of the electric field strength and electric potential for Realistic Cell_A exposed to the low-frequency electric field: a) the spectrum of equipotential lines and electric field strength related to the amplitude of the applied electric field 10^5 V/m; b) detailed view in the vicinity of the cell - color map and arrows; c) detailed view in the membrane and its vicinity [23]

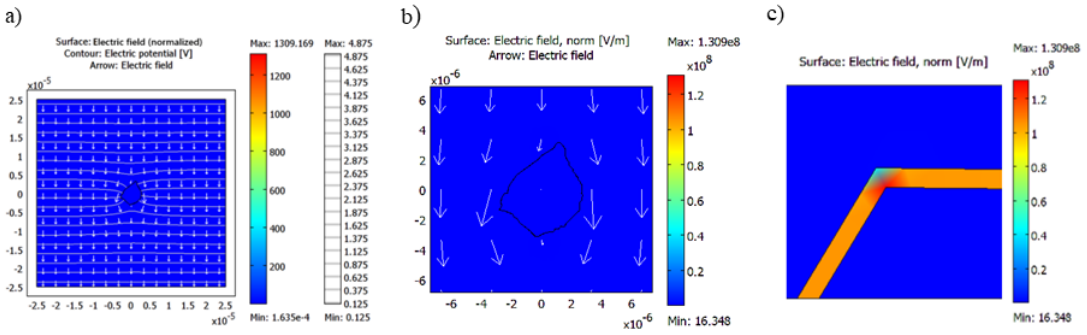

Fig. 5.6 Distribution of the electric field strength and electric potential for Realistic Cell_B exposed to the low-frequency electric field: a) the spectrum of equipotential lines and electric field strength related to the amplitude of the applied electric field 10^5 V/m; b) detailed view in the vicinity of the cell - color map and arrows; c) detailed view in the membrane and its vicinity [23]

By exposing the cells to a low-frequency electric field, it was observed that the cytoplasm behaves as a conductive material compared to the insulating membrane, so that the induced electric field inside the cell is negligible compared to the level of the field outside it (as shown in Fig. 5.5 and Fig. 5.6). To highlight even more the influence of cell shapes on the distribution of the electric field and the induced transmembrane voltage, two circular models were associated with realistic ones. The Realistic cell_A was associated with the Circular cell_A with a radius of 5.28 μm, and the Realistic cell_B was associated with the Circular cell_B with a radius of 2.9 μm (Fig. 5.7). The radii are determined by equating the areas of the corresponding 2D domains.

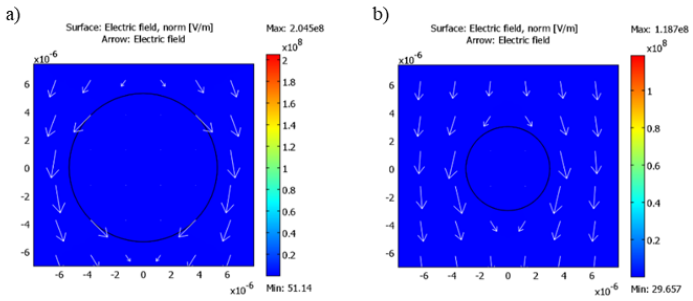

Fig. 5.7 Distribution of the electric field strength for circular cells exposed to the low-frequency electric field: a) Circular cell_A; b) Circular cell_B

The differences that are observed in the spectrum of the electric field affected by the presence of exposed cells and dependent on the shape and size of the cells, also have consequences on the control indicator for electroporation-induced transmembrane voltage (ITV). ITV has maximum values in the polar areas of the cell (areas for which the vector **E** is normal at the membrane surface).

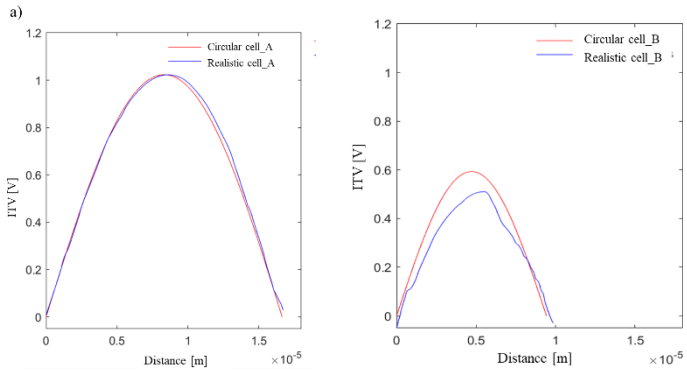

Fig. 5.8 ITV amplitude (absolute value) on half of the cell contour for the corresponding cell models (A and B respectively): a) Circular cell_A and Realistic cell_A; b) Circular cell _B and Realistic cell_B

From Fig. 5.8a) it can be seen that by superimposing on the same graph the membrane stresses the differences between the Circular cell _A and the Realistic cell_A are quite small, due to the similarity in shape. Whereas in the case of overlapping Realistic Cell_B with Circular Cell _B, Fig. 5.8b), the differences are more obvious, due to its irregular shape.
It is observed that the cells with a more irregular shape and several sharp parts determine the concentration of the electric field, a useful observation for detecting areas favorable to the phenomenon of electroporation. It is thus expected that a correlation between the orientation of the **E** vector and the realistic cell positioning (with the surface having smoothness deviations) can lead to maximums in the ITV values depending on the cell position, i.e. regions of the membrane preferentially exposed to electroporation.

5.4 STUDY OF A REALISTIC CELL MODEL AT DIFFERENT POSITIONS AGAINST THE ORIENTATION OF THE APPLIED ELECTRIC FIELD AT LOW FREQUENCY

In the present study, the influence of cell orientation on a low frequency (1 kHz) electric field for a realistic ellipse-shaped cell was numerically addressed Fig. 5.9.

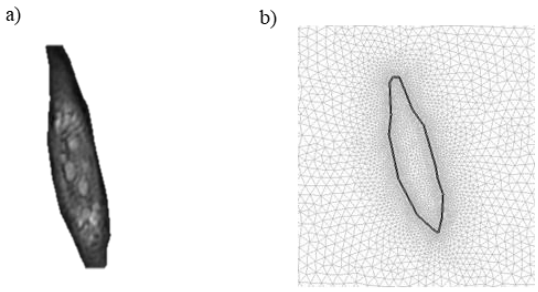

Fig. 5.9 Realistic cell_C: a) Phase image reconstruction; b) Cell imported in Comsol and mesh

Fig. 5.9 shows the Realistic cell_C oriented with the large axis at several degrees, going through a complete rotation starting from 0^{o} degree between its axis and the direction of the intensity vector of the applied electric field.

From the electric potential spectrum (Fig. 5.10) it can be seen that the intensity of the electric field is more concentrated in the extremities of the cell (north pole and south pole), so that ITV reaches maximum (respectively minimum) values in these areas. In all cases, the values of the induced transmembrane voltage (on the circumference of the cell) remain in the range of -0.8, 0.8 V approximately. The location of the maximum (or minimum) values is associated with the membrane areas that are placed at the poles, even if they represent for each position other membrane areas of the rotating cell.

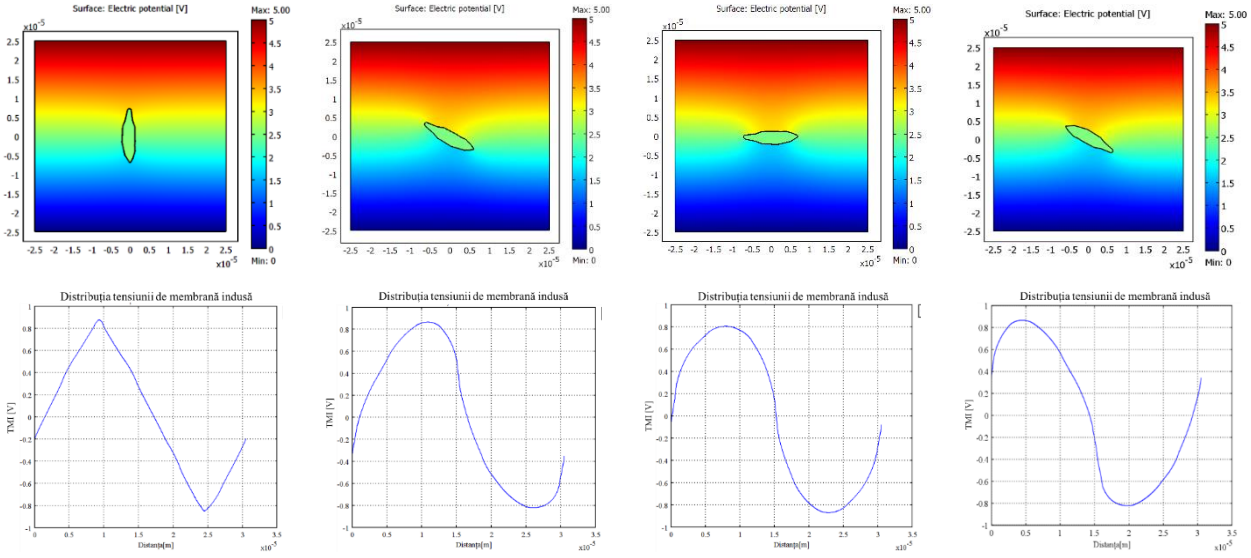

Fig. 5.10 Influence of the applied electric field on an elongated cell, at several degrees of rotation of its axis with the direction of the applied vector **E** (E = 1kV / cm, f = 1 kHz); for each position were represented: the electric potential in the color spectrum (top) and the ITV distribution on the cell contour (bottom)

To analyze whether the shape of the contour influences the ITV values, we fixed a point on the cell membrane and followed the ITV values at this point, as the cell orientation in the field changes (within 0º and 330º degrees between the major axis of the cell and field lines). This study was performed for two fixed points of the contour: from the smooth area (point 1) and the sharp area (point 2) of the cell, according to Fig. 5.11a), and the values were shown in Fig. 5.11b) and Fig. 5.11c). It is observed that the induced transmembrane voltage has values between -1V and 1V in both cases; the positive and negative maxims, are reached when the chosen point passes through the pole area. We can say that the values of ITV at a certain point, are insignificantly dependent on the shape of the cell, the local curvature, and the deviations of the membrane from the smoothness, instead, it strongly depends on the orientation of the cell as a whole to the field lines. The values reached by the ITV are slightly different in the area of the local peaks from the areas in the immediate vicinity, according to the representations of the electric field strength spectrum in chapter 3.

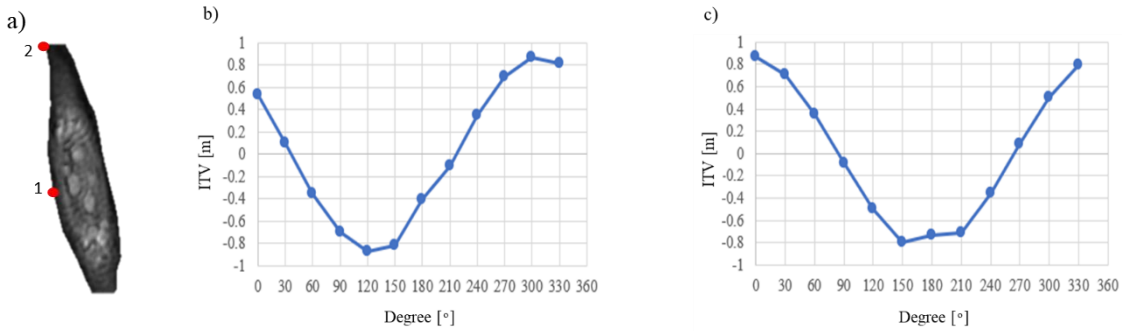

Fig. 5.11 Maximum values of ITV at two points on the membrane surface, taken as landmarks, at a complete rotation of the elongated cell in a uniform low-frequency electric field: a) Landmarks fixed on the cell contour; b) Maximum ITV values at the control point (1) at a complete cell rotation; c) Maximum ITV values at the control point (2) at a complete cell rotation

5.5 STUDY OF THE INFLUENCE OF FREQUENCY ON THE INDUCED TRANSMEMBRANE VOLTAGE

This study was performed to determine the dependence between the distribution of electric field around the cell, respectively between the induced transmembrane voltage and the frequency of the applied electric field (within the harmonic or continuous-wave regime); a significant parameter for results is given by the morphological features of the analyzed cell, i.e. the shape and size of the cells. The comparison concerns the two types of realistic cells previously modeled - type A and type B - different in shape and size, exposed in similar conditions (harmonic electric field with the same amplitude and frequency), for a frequency range between 10 kHz -10 GHz.

The realistic cell models were initially exposed to a low-frequency (10 kHz) harmonic electric field, then to a high-frequency (1 GHz) with an intensity of 1 kV/cm. Fig. 5.12 and Fig. 5.13 show the distribution of the electric field strength (color spectrum for values related to the amplitude of the applied field) and the equipotential spectra at low-frequencies (Fig. 5.12), respectively at high-frequencies (Fig. 5.13). By comparing the images Fig 5.12a) with Fig.5.13a) and Fig. 5.12 b) with Fig. 5.13b) one can see the significant differences between the impact that the electric field has on the cells at low and high frequency. The shielding effect that the membrane has against the penetration of the electric field inside the cell at low-frequencies is almost invisible at high-frequencies. At the same time, the electric field strength at the membrane level is considerably lower at high-frequencies than at low-frequencies (more than an order of magnitude) for the same amplitude of 1 kV/cm of the applied field. If we relate these observations to the effect of electropermeabilization, we could deduce that the amplitude of the applied electric field should be increased accordingly, with the increase of the applied electric field. The results obtained numerically are following the conclusions of the theoretical and experimental investigations presented in the literature [54], [22], [58].

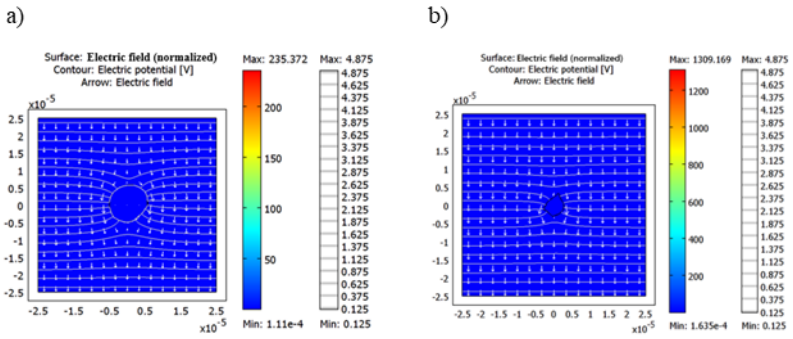

Fig. 5.12 Equipotential lines and electric field strength (color map and arrows) at low-frequency (10 kHz); E-values are rated to 10^5 V/m, the amplitude of the initial uniform field: a) Realistic cell_A; b) Realistic cell_B [23]

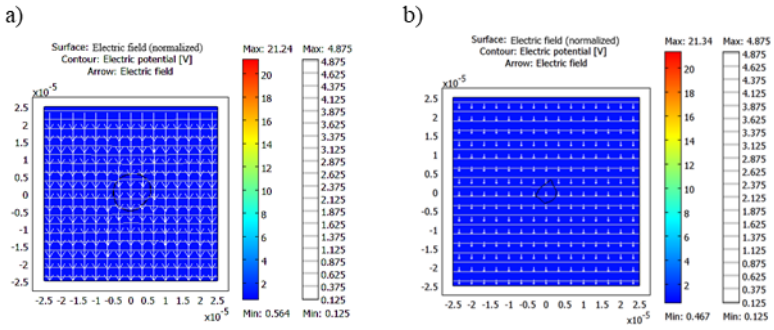

Fig. 5.13 Equipotential lines and electric field strength (color map and arrows) at high-frequency (1 GHz); E-values are rated to 10^5 V/m, the amplitude of the initial uniform field: a) Realistic cell_A; b) Realistic cell_B [23]

By exposing the cells to a uniform low-frequency electric field compared to the high-frequency one were observed different behavior of the cells, Fig. 5.14. At low-frequency, the ITV values are about two orders of magnitude larger than the high-frequency values for the same amplitude of the applied electric field. It can also be seen that the irregular shape of the cells causes deviations from the idealized case (perfectly sinusoidal shape present in the case of circular cells), the phenomenon being more pronounced at high-frequencies.

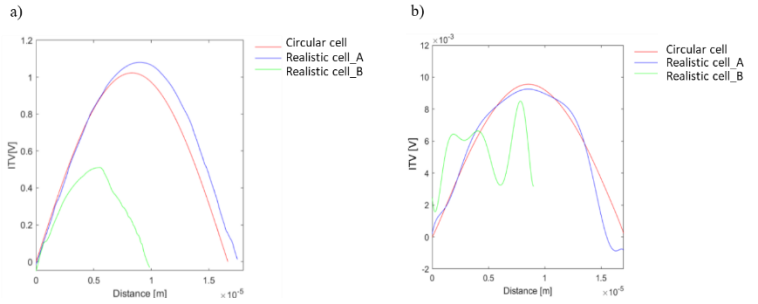

Fig. 5.14 ITV amplitude (absolute value) on half of the cell contour for three cell models: Circular cell_A, Realistic cell_A, and Realistic cell_B subjected to the same electric field of 1 kV/cm: a) low-frequency (10 kHz); b) high-frequency (1 GHz) [23]

Starting from these observations, we continued the study of the penetration of the electric field inside the Realistic cells A and B by comparing with the Circular cells A (radius 5.28 μm) and B (radius 2.9 μm) for the whole frequency range 10 kHz - 10 GHz. From Fig. 5.15 can be observed the frequency dependence of the maximum values of the induced transmembrane voltage, with the same tendency for all cell morphologies, determined by the electrical properties of the membrane. The properties of the other components of the cell have a smaller impact on the distribution of electric field sizes for the high-

frequency range. In the case of low-frequencies (JF) the electrical properties provide insulating characteristics to the membrane, and the amplitude of ITV is almost constant for values < 100 kHz. In the 100 kHz to 10 MHz range, medium-frequency (MF), the ITV amplitude decreases by two orders of magnitude and remains constant at > 10 MHz, the high-frequency range (HF).

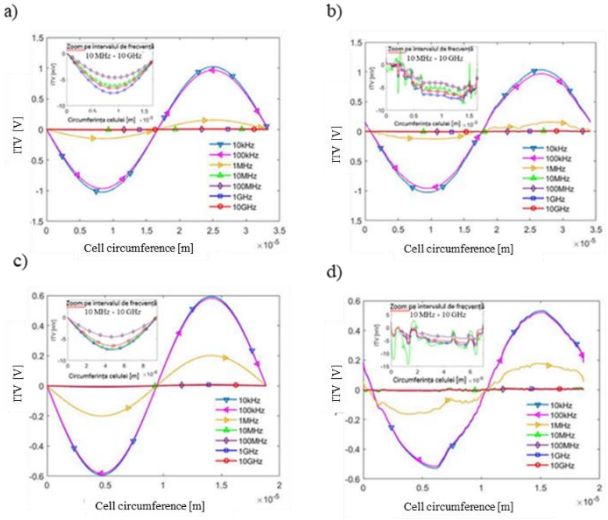

Fig. 5.15 ITV along the entire contour of each analyzed cell, under uniform E-field (CW, 1kV/cm); field frequency is a parameter of the study in the range 10 kHz - 10 GHz: a) Circular cell_A; b) Realistic cell_A; c) Circular cell_B; d) Realistic cell_B [24]

Fig. 5.16 illustrates the frequency dependence of the maximum value of the induced transmembrane voltage (ITV_{max}), identified and calculated in the upper region of each cell on the whole frequency spectrum, 10 kHz - 10 GHz (left image) and an enlarged frequency range tall (right image). The analysis of the graphs shows a similar trend for all cell morphologies because the frequency dependence of ITV_{max} values is mainly determined by the electrical properties of the membrane, which gives insulating characteristics to the membrane at low-frequencies, but by increasing frequency, these characteristics are lost.

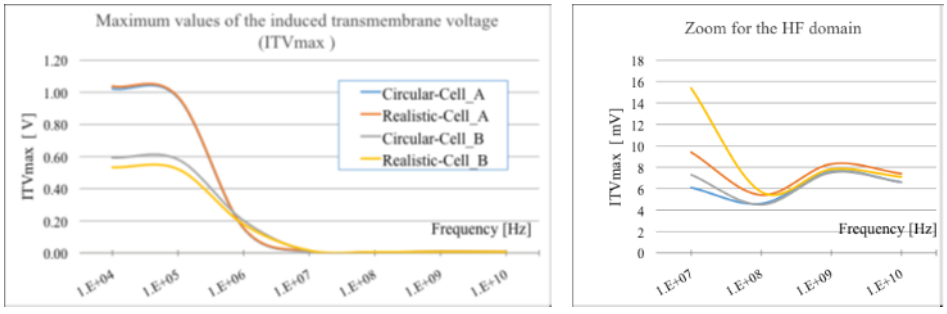

Fig. 5.16 ITV_{max} variation with the frequency of the applied electric field (CW, 1kV/m uniform field) for the four analyzed morphologies (two realistic and two circular samples, and respectively two size categories). ITV_{max} over the entire frequency range (left) and magnified in the HF domain (right) [24]

5.6 STUDY OF THE BEHAVIOR OF A GROUP OF CELLS IN THE ELECTRIC FIELD; THE INFLUENCE OF DISTANCE BETWEEN CELLS ON THE INDUCED TRANSMEMBRANE VOLTAGE

Under natural conditions, cells are rarely isolated, and the density of cell solutions and the placement of cells relative to each other are factors that in turn influence the distribution of the applied

electric field. Most often the cells are in direct contact, thus forming two-dimensional monolayers (monolayers attached to the bottom of a vessel), or three-dimensional (tissues), or even interconnected.
This subchapter follows on from the previous ones in which, over a large frequency range, the effects of the electric field applied on the single cells in a realistic shape compared to the circular ones and the ITV levels likely to produce the electroporation process were studied [23], [24] and aims to study cell suspensions exposed under similar working conditions.

The numerical models made in this case consist of idealized groups of cells (circular, identical, and placed in an orderly controlled manner) that have been exposed to a harmonic electric field over a wide range of frequency variation, covering the three areas specified above: low (f < 100kHz), medium (100 kHz < f < 100MHz) and high-frequency (100 MHz < f < 10 GHz). It was followed by how various parameters, such as the distance between the cells, the position inside the enclosure, the frequency of the electric field, etc. influences the maximum values of ITV [112].
In the cases presented below, idealized matrices of distinct cells were considered, which do not touch each other and are positioned in an orderly manner, at distances that can vary, suggesting variations in the density of the cell-matrix. The configuration has similarities to a low-density cell preparation. For this study, idealized cells of circular shape, with a radius of 5 μm (similar to the idealized cases presented previously in chapter 4 and used for the studies in 5.2 and 5.5) were considered. The minimum distances between the cells were varied in the range (0.1… 9) μm. The study was performed considering the exposure to a harmonic electric field, with variable frequency in the range 10 kHz… 10 GHz; cytoplasm and intercellular fluid are relatively good conductive media, with similar electrical properties, and the membrane is a lossy dielectric medium with significantly dependent frequency conductivity and dielectric constant (Debye models presented in subchapter 5.2 with data from [101]). In all the cases studied and presented below, the applied electric field was maintained at E = 1 kV/cm, a condition that allows the comparison on a common basis of all the analyzed cases.
Two configurations were analyzed:
(a) a matrix of five identical cells, structured as follows: a central cell and four cells arranged symmetrically around it (marginal cells), positioned in directions 45º from the direction of the vector **E** applied.
(b) a matrix of seven identical cells, structured as follows: a central cell and six cells arranged symmetrically around it (marginal cells), positioned in the parallel direction, respectively in directions oriented 30º from the direction of the vector E applied.

Fig. 5.17 and Fig 5.18 shows the two configurations and the solutions of the electric field problem at two frequencies representative for the LF (10 kHz) and HF (1 GHz) - the electric potential in color map and equipotential lines, over which is superimposed the electric field strength in representation with arrows. It is observed that the distributions of electrical quantities are generally influenced by frequency similar to the cases studied in subchapter 5.5 for a single suspended cell. The differences between the corresponding cases are mainly explained by the variation with frequency of the electrical properties of the cell membranes.

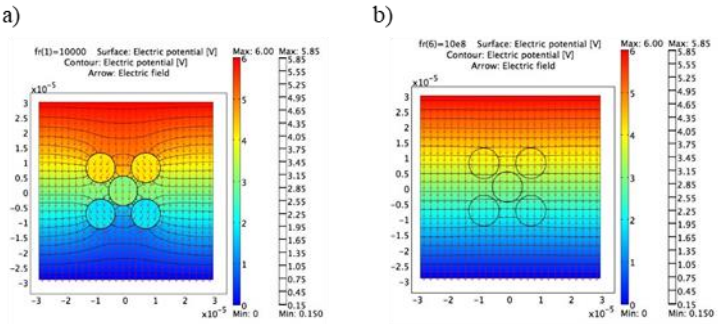

Fig. 5.17 Distribution of electric potential (color map and equipotential lines) and electric field strength for an array of **five** identical cells, positioned in directions 45º from the direction of the vector **E** applied: (a) frequency 10 kHz; (b) 1 GHz frequency

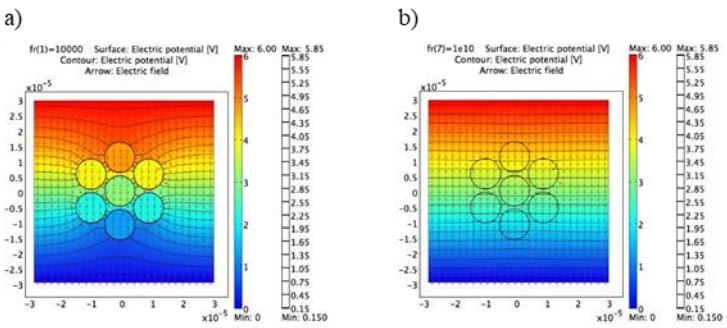

Fig. 5.18 Distribution of electric potential (color map and equipotential lines) and electric field strength for an array of **seven** identical cells, positioned in directions 30º from the direction of the vector **E** applied: (a) frequency 10 kHz; (b) 1 GHz frequency

Analyzing the dielectric stresses (ITV_{max} values) in different cases, it is observed that notable differences between configurations (both from one cell to another and from one matrix density to another) appear only at low-frequencies (f < 100 kHz). In contrast, at high-frequencies (f > 100 MHz) all cases analyzed show very close dielectric stress levels, regardless of the matrix density or the position of the cell as a whole matrix. These high-frequency values (ITV_{max} values) are, however, approx. an order of magnitude compared to that observed for a single suspended cell (approx. 0.1 V versus 0.01V).
Figures 5.19-5.20 show families of ITV_{max} control size curves across the range of frequencies relevant to electroporation; the cases of the matrix of **five** and **seven** cells are analyzed, with the identification of ITV_{max} values separately for the central cell and a lateral cell. The parameter of the curve family is the distance between the cells, measured in the area where they are closest, and values in the range of 0.1 µm ... 9 µm are taken into account. It is thus considered that the cells remain in suspension without touching, which corresponds to the case of relatively low densities. ITV_{max} refers to the highest point values of membrane voltage induced by exposure in the electric field, values recorded at the cell poles, or in the area on the surface of a cell where the normal component of the vector **E** is maximum.

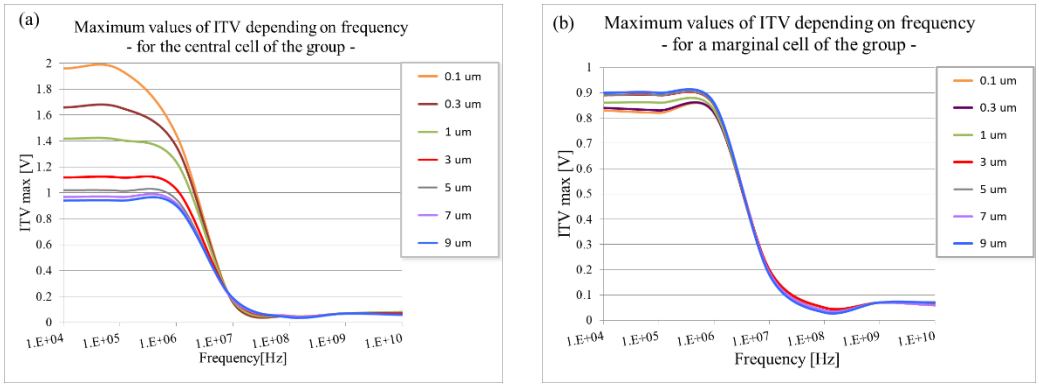

Fig. 5.19 ITVmax variation with the frequency of the applied electric field (CW, 1kV/m uniform field) for different distances between the cells of the configuration with **five** identical cells: a) the central cell; b) a marginal cell

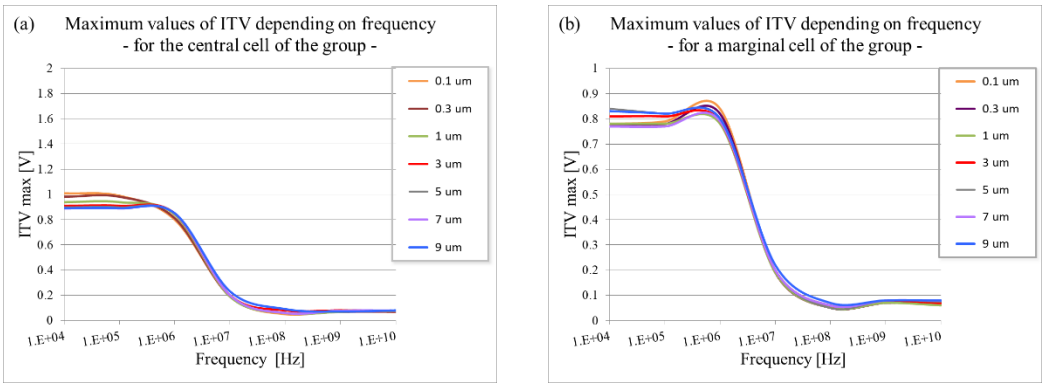

Fig. 5.20 ITVmax variation with the frequency of the applied electric field (CW, 1kV/m uniform field) for different distances between the cells of the configuration with **seven** identical cells: a) the central cell; b) a marginal cell

CHAPTER 6
NUMERICAL MODEL FOR PORE FORMATION - EXPOSURE TO PULSED ELECTRIC FIELD

The objective of the study is to develop a numerical model for analyzing pore dynamics and validating the results obtained, by comparison with experimental data from the literature, the permeability percentage in [113], and the median fluorescence in [115].

To carry out this study, a 2D model with axial symmetry of a spherical cell placed in a cylindrical enclosure was created to be exposed to a pulsating electric field, which allows the simulation of bipolar pulses, with adjustable parameters (duration, frequency repetition). The calculation domain and the boundary conditions were established according to Fig. 6.1, where V0 represents the applied electric potential in the form of a train of 50 bipolar pulses; each pulse having a duration (T1) of 1 μs, with a pause interval, T2 between pulses. The duration T2 of maintaining the value V0 = 0 between the two pulses is an important parameter in the numerical modeling of the pore formation phenomenon, and the analysis presented below considers the cases in which T2 takes the values of 1 μs and 10 ms respectively.

Fig. 6.2 shows the general waveform, applied to represent the variation of the potential V0, i.e. the function V0 (t) used in the calculation model.

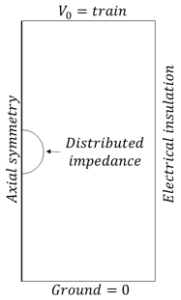

Fig. 6.1 Calculation domain and boundary conditions

The numerical model was applied for several cases according to the two values of the pause interval, T2 and the electrical conductivities of the extracellular environment, and for each case, the local pore density was calculated at different values of electric field strength, between 0… 5000 V/cm. The electrical properties were taken from [113] and [123].

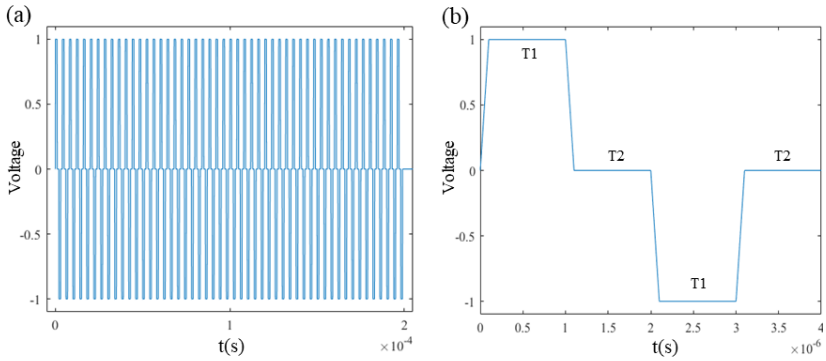

Fig. 6.2 Numerical modeling of short bipolar pulses. (a) One burst consisted of 50 bipolar pulses. (b) Each bipolar pulse consisted of a positive and a negative pulse, both of length 1 μs (T1) and the inter-phase delay and inter-pulse delay of 1 μs (T2). During our simulation, T2 was either 1 μs or 10 ms. The rise time and fall time for each pulse were 100 ns [125].

Fig. 6.3 represents the pore formation through the cell membrane, in the extracellular environment with low conductivity by exposing it to different maximum values of the electric field, in the range 0… 5000 V/cm, having an incremental step of 1000 V/cm. This figure highlights all the stages of electropermeabilization of the cell membrane by creating pores after applying the external electric field. Therefore, from the linear scale representation, one can observe the phase of resealing the pores, implicitly from the regeneration of the membrane, after reaching the maximum number of pore formation, while from the logarithmic scale representation one can observe the initial stages of pore formation (initiation, expansion and partial recovery). By applying this model it is observed that the density of the pores increases in proportion to the intensity of the applied electric field.

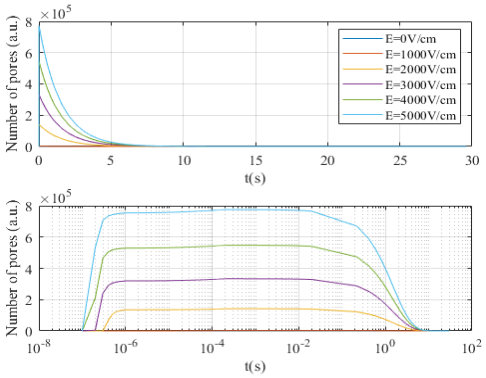

Fig. 6.3 Number of pores as a function of time for different values of the applied electric field in low conductivity buffer for one burst of 50 bipolar pulses, each pulse with the duration of 1μs and inter-phase delay of 1 μs. (a) In a linear scale we can observe the dynamics of pore resealing; (b) In a logarithmic scale we can observe the initial steps of pore formation [125].

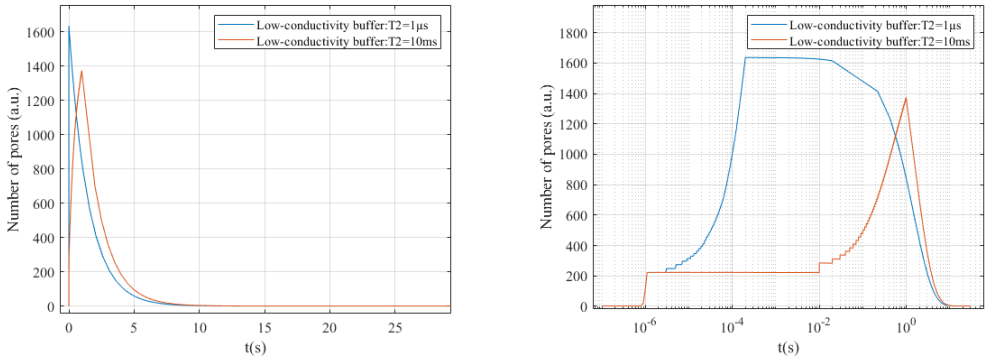

Fig. 6.4 Number of pores as a function of time for two different inter-phase delays (T2), either 1 μs or 10 ms, in low-conductivity buffer at 1 kV/cm; (a) In linear scale, we can focus on the pore resealing; (b) In a logarithmic scale, we can focus on initial pore formation during the burst application [125].

Fig. 6.4 represents the evolution of the number of pores as a function of time, for the two cases of considering the pause interval T2 between pulses, 1 μs, and 10 ms respectively, and the cell is placed in the extracellular environment of low conductivity, following the application of an electric field with a maximum current of 1 kV/cm. From the logarithmic representation (Fig. 6.4b) one can observe the gradual increase of the number of pores, for T2 = 10 ms, compared to the abrupt increase when T2 = 1 μs. However, in the case of T2 = 1 μs, a larger number of pores were obtained, which remained open for a longer time, in contrast to the case of T2 = 10 ms.

For validation, we initially compared the numerical results with the experimental ones from [113] where the percentage of cell permeability was analyzed. Experimentally, the authors of [113] found that the maximum number of permeabilized cells was reached after applying a certain electric field, while from our results obtained by numerical modeling (Fig. 6.5), we observed that, by increasing the electric field, the number molecules entering the cell (molecular absorption) continued to grow. The higher the amplitude of electric fields applied to the cells, the higher the molecular absorption, even if the maximum number of permeabilized cells has been reached experimentally. Thus, on a linear scale, the increase of the AUC value is also linear at low amplitudes of the electric field strength. Following this observation, we decided to extend the study by comparing the numerical values with the median fluorescence of propidium iodide in [115].

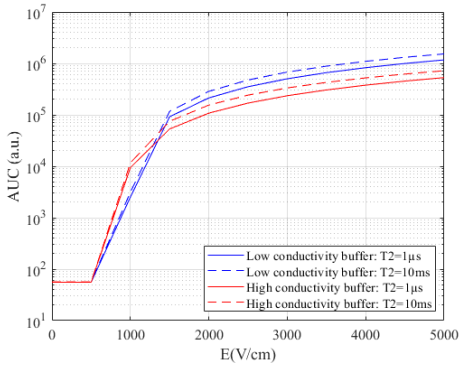

Fig. 6.5. Area under the curve as a function of the applied electric field in low and high-conductivity buffers for one burst of 50 bipolar pulses. Pulse duration (T1) was 1 μs, and the inter-phase delay (T2) was either 1 μs or 10 ms. In the linear scale, the AUC value increases linearly [125].

After superimposing on the same graph the experimental values (median fluorescence) and the numerical ones (pore formation) we noticed that is a similarity between them of the tendency to increase the absorption even after reaching the maximum number of electroporated cells at 3500 V / cm (Fig. 6.6).

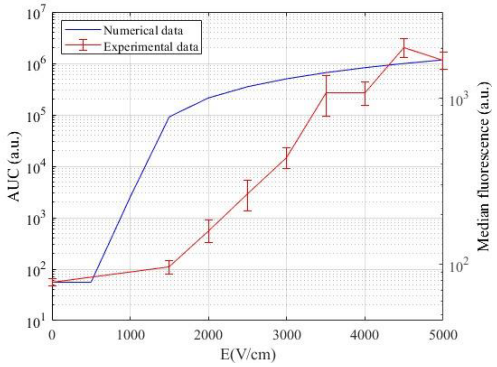

Fig. 6.6 Comparison of measured and simulated molecular uptake based on fluorescence and pore formation. The measured values are shown as a mean ± standard deviation and were obtained from [115].

From the numerical results, it was observed that the density of the pore number has the same tendency of increase proportional to the amplitude E for both values of extracellular conductivity. However, by comparing the numerical results with the experimental ones from [113] it was observed that the molecular absorption behaves differently for the two types of the extracellular environment. For the extracellular medium with high conductivity, the numerical results are similar to the experimental ones in [113]; but for the extracellular environment with low conductivity, the numerical model does not provide satisfactory results, which means that there is a difference between the two environments, probably related to the biology or chemistry of the electroporation phenomenon that was not included in the numerical model.

The differences between numerical and experimental values are due to the limitations of the numerical model. First, to reduce computation time and resources, a single train of 50 bipolar pulses was modeled, instead of eight, as experimentally applied. Secondly, the numerical model does not include the enlargement or reduction of pores and thirdly, the transport mechanisms (electrophoresis and diffusion) were not taken into account. It has been assumed that the number of pores is correlated with transport, i.e by increasing the number of pores, transport increases, and was approximated by calculating the value of the area under the curve (AUC).

CONCLUSIONS

C1. GENERAL CONCLUSION

Particular attention was paid, in the research program presented in the thesis, to the aspects of correlation of the different parameters characteristic of the EP process, on the one hand, details related to the variety of cellular structures and on the other hand, the parameters of the applied electric field. In the preparation of the experiments, an essential step is to identify the domains of variation of the parameters that the researcher has at his disposal to diversify the analyzes considered and the domains of values of the variables explored. Thus, in preparing a study, the stage of establishing the appropriate settings for the laboratory experiment or numerical simulation should be covered.

The study presented in the thesis is based on consistent documentation in the literature, with contributions beginning from the 1950s with studies of analytical modeling of idealized shapes of spherical cells in the electric field (Schwan models) and the study of electrical properties of cell components. In the last 2-3 decades, the literature in the field has been spectacularly enriched in several main directions: (1) laboratory analysis, based on controlled electrochemical experiments of

transmembrane transport phenomenon; (2) analysis by numerical simulation of electric field problems, associated with the simulation of the pore generation phenomenon, either by statistical models or by nonlinear dynamics that try to explain the physico-chemical changes at the level of elementary particles in the structure of membranes.

One of the centers of research acknowledged at the international level for consistent results and a study carried out over a long period, is the Laboratory of Biocybernetics at the Faculty of Electrical Engineering, University of Ljubljana, where I took part in a collaborative program as a visiting student, where I had the opportunity to collaborate with colleagues on a project to simulate pore generation statistics, which is presented in Chapter 6 of the thesis.

This thesis presents several studies on the numerical modeling of the phenomenon of membrane electropermeabilization and its usefulness in bio-medical applications starting from simple models of spherical cells to realistic-shaped models of cells obtained by optical microscopy. Numerical simulations were performed using the finite element method (Comsol Multiphysics software). The experimental acquisition of cellular images was performed by holographic and dark-field microscopy techniques, and the preprocessing of these images representing realistically shaped cells was performed with the specific software for each microscope. For the representation of images as computational domains in Comsol Multiphysics, the processing was performed in several stages: with MATLAB software for cell segmentation and AutoCad for selecting the limits of cell shapes and establishing the thickness of the cell membrane.

Chapter 1 presents an analysis of the literature and the general elements of the electroporation phenomenon and its applications; the studied literature fully proves that electropermeabilization is a topical field, intensively studied by researchers. We have also noticed over time an increase in interest in numerical modeling of both single realistic cells and multiple cell structures, as this is an economical way to test various parameters used experimentally, thus increasing the efficiency of applied electroporation technologies. particularly in various bio-medical interventions. From this study, was observed that there are several objectives aimed at researching this phenomenon: (1) analysis of the electrical stress to which the cell membrane is subjected which makes it possible to increase the membrane voltage and the probability of triggering the electropermeabilization process; (2) the dynamics of pore formation by applying a pulsed electric field, (3) continuous-wave excitation, the spectral analysis of which is considered more accurate due to the narrow bandwidth.

Chapter 2 presents the experimental aspects specific to membrane electropermeabilization: the equipment used and their classification, the physical characteristics of the cells, the parameters of the external electric field, and the environmental conditions. The parameters used in the simulations refer to the dimensions and shapes of the cells, the thickness of the membrane, and the electrical properties of the material for each cell component. A syntesis was made, concerning the sets of values resulting from experimental tests and used in research for the construction of analysis models by numerical simulation; two documentary studies were conducted on the morphological characteristics of the cell and the environmental electrical properties specific to the cell structure.

Chapter 3 shows the principles of recording biological samples by two optical methods: digital holographic microscopy (DHM) and dark-field optical microscopy for hyperspectral and 3D imaging, their advantages, and their applications. Were studied and used these two techniques in the acquisition of images of different types of cells in cultures to use them for further processing and to extract information by calculating specific parameters. Digital holographic microscopy, being a technique dedicated to the study of transparent, phase samples, found in their natural environment, without the need for fluorescent labeling, was used to record cells during and after the application of electroporation pulses. This is possible because DHM does not use scanning during experimental recording, resulting in the advantage of acquiring images of fast phenomena in real-time. Dark-field microscopy due to the high resolution on the 3 axes were used to record and acquire cell images on compartments (cytoplasm and nucleus). In the case of each technique, were successively presented all the steps used in the process of recording, acquiring, and processing the images, until obtaining the 3D reconstructions of the cell structures; they are exported to the suitable software for the description of the electric field problem. Comsol

Multiphysics based on the finite element method was chosen here to analyse the exposure of cell structures to the electric stress.

Chapter 4 consists of validating the main characteristics involved in formulating numerical models of cell exposure to a uniform electric field, by comparing the basic results with data from analytical calculations in literature. Initially, were described the homogeneous and inhomogeneous analytical models of a spherical body in a uniform electric field framed in the spherical and Cartesian coordinate system. Then analyzed the results obtained with the inhomogeneous model by creating three numerical models, the first model created being the 3D one, which is the most similar to the analytical model. Starting from this we built, by applying symmetry criteria, two other 2D models: a) The 2D - axial model, based on axial symmetry in polar coordinates, which represents the natural reduction of the 3D structure, and b) the 2D - Cartesian model constructed as a representation of a cross-section through the whole cell, in Cartesian coordinates. Each model was implemented and studied in time harmonic low frequency operating mode, the comparative analysis supports the validation of an operational, working model, used later in the numerical simulation study where the results obtained (distribution of electric field intensities inside and outside the cell and the value of the induced membrane voltage ITV) were compared with data produced by the analytical model taken as reference. Since all three numerical models produced results comparable to each other and to the reference analytical model, was concluded that the 2D-Cartesian model can represent the behavior of realistic cells in an acceptable way and with accuracy comparable with other models. It was shown that the 2D - Cartesian model could be used in applications based on the technique of digital holographic microscopy (MHD), which provides images for suspended cells, suitable to form the basis of the construction of computational models for the analysis of electric field problems with the finite element method.

In Chapter 5 was performed numerical modeling of realistic cellular structures of various shapes and sizes obtained by digital holographic microscopy (MHD).

A first study was the influence of cell membrane thickness on membrane voltage induced by the application of a low-frequency electric field. The study was performed on numerical models of some spherical cell structures, compared to the realistic ones. The cell membrane thicknesses ranged from 5 nm to 100 nm. From the obtained results it was found that the induced transmembrane voltage at low frequencies is not significally influenced by the thickness of the membrane, although in the case of realistic cells there are small variations due to irregular shapes. But even in these cases, the distribution of the induced transmembrane voltage is, by analogy with the case of spherical cells, very close to the shape of a sinusoid (or cos-sinusoid) obtained for spherical models. From here it was found that numerical models can be made for realistic cellular structures with larger membrane thicknesses, to shorten the processing time and save computing resources. Also in this case we noticed that the induced membrane voltage is influenced both by the shape of the cells and by their characteristic size according to the orientation of the electric field; therefore the following study was related to the determination of ITV, as well as the distribution of the low-frequency electric field.

Exposure of a cell to a uniform low-frequency electric field inside an enclosure disrupts the uniform distribution of the initially applied field and depending on the electrical properties of the cellular components, the electric field may be concentrated in different areas of the cell. Due to the low electrical conductivity, the membrane behaves like an insulator and concentrates the electric field at its poles, and inside the cell, the field distribution is quasi-uniform, and its values tend to vanish, due to the predominantly conductive character of the cytoplasm. To highlight even more the influence of cell shapes on the distribution of the electric field and the induced transmembrane voltage, we made two models for idealized circular cells, each associated with a realistic cellular configuration, of approximately equal dimensions. By comparing the results, we noticed that the more irregular the shape of the cells and the more sharp parts, the electric field is more concentrated in those areas, a useful criterion for detecting areas favorable to the initiation of electroporation.

After exposing realistic cells and the associated circular patterns to a low frequency (10 kHz) harmonic electric field with an amplitude of 1 kV / cm, we continued the study to see the dependency between the induced membrane voltage and the frequency of the applied electric field, for a range of

frequencies between 10 kHz - 10 GHz. By comparing the results obtained for each cell type, we noticed significant differences in the impact that the electric field has on the cells at low and high frequencies. The net shielding effect of the membrane at low frequencies against the penetration of the electric field inside the cell is almost non-existent at high frequencies. At the same time, electric field strength inside the membrane is lower by an order of magnitude at high frequencies than at low frequencies for the same intensity of the applied electric field (1 kV / cm). Regarding the values of the induced membrane voltage, we noticed that at low frequencies, they are about two orders of magnitude higher than the values corresponding to the high frequencies for the same intensity of the applied electric field.

We also studied the dependency of ITV on the orientation of a realistic cell with an ellipse-like shape in the applied low frequency 10 kHz electric field. For this study we rotated the cell with the large axis at several angles, going through a complete rotation, starting from an angle of 0 ° between its axis and the applied electric field. From the color spectra of the electric potential, it was observed that the intensity of the electric field is concentrated more in the extremities of the cell (north pole and south pole, respectively, where equipotential lines thicken, causing a large gradient) and extreme values (maximum positive and negative respectively) of the induced membrane voltage is associated with the membrane areas placed at the poles, regardless of the angle of rotation of the cell. A systematic study of ITV values found that the values of the membrane voltage induced at a certain point do not depend significantly on the shape of the cell membrane in that place, but on the orientation of the cell as a whole relative to the field lines.

Another study was represented by the effects of the electric field applied on some groups of cells with idealized shape (cell-matrix) aiming to determine the rules of behavior of cell suspensions in terms of dielectric stress favorable to electroporation. The indicator of the highest dielectric load is considered to be the maximum value of the induced membrane voltage (ITVmax) that can be associated with the trigger threshold of electroporation because it is proportional to the intensity of the applied electric field but also depends on the field frequency and the presence of other. neighboring cells. In this case, we followed how various parameters such as: the distance between the cells, their position inside the enclosure and the frequency of the applied electric field, influence the value and distribution of the induced membrane voltage. We analyzed by comparison the configurations and implicitly different densities of the group of identical cells in suspension, evaluating the influence of the density of the solution (respectively of the distance between the cells) and the central or marginal position of a cell within the configuration. After analyzing the dielectric stresses (ITVmax values) we noticed noticeable differences between configurations (both from one cell to another and from one matrix density to another) only at low frequencies (f < 1 MHz). Whereas, at high frequencies (f > 100 MHz) it was observed that the dielectric stress levels are very close, regardless of the density of the matrix or the position of the cell in the whole matrix, although the ITVmax values were higher by approx. an order of magnitude compared to those observed for the case of a single suspended cell. Regarding the results obtained by original modeling and analysis, it can be said that they correlate well with the trends and behaviors reported in general in the literature, in the experimental and simulation studies we have researched.

In Chapter 6 we analyzed the electroporation process by numerical modeling of the pore formation dynamics when applying a train of 50 bipolar pulses with duration T1 = 1 μs, having a pause interval between phases, T2 = 1 μs and 10 ms respectively and we validated the results obtained with experimental results from the literature. We worked with maximum values of the electric field, between 0 ... 5000 V/cm, with an incremental step of 1000 V/cm, for two extracellular environments with different conductivities (low and high values, respectively) taken from the literature. The temporal evolution of the number of obtained pores was quantified by integrating in time the pore density function. Following the analysis of the numerically obtained values, we observed how the pore density varies with the increase of the pause interval T2 between pulses, as well as with the intensity of the applied electric field. Thus, for field values up to 1500 V/cm, a linear increase was observed, while for values > 1500 V/cm, this increase was more attenuated because the conductivity of the membrane tends to stabilize and the pore formation begins to reach a saturation process.

To validate the numerical model, we initially compared the numerical results with the percentage of cell permeability, from which we observed that by applying electric fields with higher intensities, the number of molecules entering the cells increases, even if experimentally, we reached the maximum number of permeabilized cells. The conclusions drawn from the comparison of the numerical simulation results with the experimental observations allow the identification of some deficiencies or excessive idealizations in the formulation of the numerical models and offer indications for their improvement.

C2. ORIGINAL CONTRIBUTIONS

Following the research carried out and the results obtained in this paper, a number of original contributions and significant personal results can be highlighted. They justify both the ongoing interest in the topic and the progress made at the end of the research program:

The realization of consistent documentation based on the specialized literature clarified a series of theoretical and phenomenological issues regarding the electropermeabilization of cell membranes, which are synthesized in a study presented in the first chapter of the thesis. Documentation based on the literature in the field has led to a systematic inventory of analytical modeling studies of idealized shapes of spherical cells in the electric field and the study of the electrical and morphological properties of cellular components.

The investigation of the electropermeabilization phenomenon (or rather, the conditions in which the exposure of the cells to the electric field is favorable to trigger this process) is done by numerical simulation. This approach required the construction of models with a high degree of simulation, accuracy, flexibility, and a first step in the original contributions is to formulate numerical models of spherical cell exposure to a uniform electric field and validate the main features by comparing results with data from analytical calculations in the literature.

The observation of the electroporation phenomenon and the identification of morphological aspects for the analysis of true cells required the study and application of the principles of recording biological samples by two optical methods: digital holographic microscopy and dark field optical microscopy for hyperspectral and 3D imaging. As part of the doctoral program, I conducted an original experimental program of optical analysis in collaboration with the staff of the Department of Biophysics and Cell Biotechnology at the University of Medicine and Pharmacy - Carol Davila and colleagues from the Institute of Laser, Plasma and Radiation Physics (INFLPR), from Măgurele, which includes two studies:

- A study conducted with images acquired by digital holographic microscopy was aimed at investigating the behavior of cells exposed to bipolar pulses of different amplitudes in experiments for electroporation. The reconstructions, as phase images, were processed to obtain values of some global parameters: the area occupied by the cell, the dry mass, the entropy, and their variations in time. To locally characterize the phase difference fluctuations in certain points of interest, we chose to calculate the correlation and autocorrelation functions. This approach by calculating the correlation and autocorrelation functions is a new method from two points of view: their calculation for the study of the local properties of electroporated cells and the application of these functions on phase images. The autocorrelation functions were calculated at three points: the point of maximum phase difference and at two points near the cell membrane, located along a line parallel to the field lines and passing through the point of maximum phase difference. These indicate that the central regions of the cell are much less affected by electroporation than those closer to the cell membrane.
- We used dark-field microscopy to study how cells in culture are distributed on a polymeric layer with areas of superparamagnetic micromagnets designed as a microarray similar to a chessboard in which there is an alternation between paramagnetic and non-paramagnetic areas. magnetic. Fibroblast cells were cultured on them and then subjected to a static magnetic field. It was observed that for the samples not exposed to a magnetic field, the incubated fibroblasts were uniformly attached to the entire surface of the matrix, without being influenced by the paramagnetic and non-magnetic areas. While, under the influence of a magnetic field of 1.3 T, they settled only in the area of superparamagnetic micromagnets. This

method can offer the possibility of manufacturing biocompatible micromagnets with well-defined geometries for optimal integration of skin grafts into tissues.

The main objective of image processing using optical analysis is the construction of original numerical models, based on realistic morphologies extracted from real cells. Image processing from shapes acquired by optical means to the construction of computational domains is necessary for the numerical modeling of realistic cellular structures of different shapes and sizes. In the numerical analysis study, characteristic stages were covered by objectives, development, and original results, most of them disseminated through scientific articles published in 2020 and 2021. Thus, the original contributions regarding the numerical simulation include the following:

- Study of the influence of cell membrane thickness on membrane voltage induced by applying a low-frequency electric field. We used numerical models of spherical structures compared to the realistic ones, and the cell membrane thicknesses were varied between 5 nm and 100 nm. Numerical results showed that the values of the induced membrane voltage are not influenced by the thickness of the membrane, even if in the case of realistic cells there were small variations due to the irregular shape. However, the distribution of membrane voltage has retained close to its sinusoidal (or cosinusoidal) shape for all cell forms. The analysis of this information found that numerical models for realistic cellular structures can be made with larger membrane thicknesses, to reduce processing time and save computing resources.
- Study of the influence of cell shape on induced membrane voltage and low-frequency electric field distribution. For this study, we used two models for realistic cell structures, to which we associated two models for idealized circular cells of approximately equal size. All the numerical models were exposed to a uniform low-frequency electric field as a result of which we noticed that the more irregular the shape of the cells and the sharper parts, the more the electric field tends to be concentrated in those areas.
- Study of the dependence between the induced membrane voltage and the frequency of the applied electric field for a frequency range between 10 kHz - 10 GHz. The same numerical models presented above were used for this study to see the impact that the electric field has on cells at low and high-frequency. The results obtained in this case showed that the values of the membrane voltage induced at low frequencies are about two orders of magnitude higher than the corresponding values at high frequencies for the same intensity of the applied electric field. The frequency dependence of the induced membrane voltage is determined by the electrical properties of the cell membrane.
- The study of a realistic cell that occupies different positions against the orientation of the applied electric field (at low frequencies) and their influence on the values of the induced membrane voltage. For this study, we used a cell with an ellipse-like shape that we oriented in a low-frequency electric field (10 kHz) with a large axis at more angles until a complete rotation. The numerical analysis found that the orientation of the cell as a whole influences the values of the induced membrane voltage.
- Carrying out a study on the effects of the applied electric field on groups of cells with an idealized shape in terms of dielectric stress. In this case, it was followed by how various parameters such as: the distance between the cells, their position inside the enclosure and the frequency of the applied field, influence the value and distribution of the induced membrane voltage. For this, we analyzed by comparison configurations with different densities of identical cells in suspension and we evaluated the influence of the distance between the cells and the central or marginal position of a cell within the configuration. The numerical results obtained in this case showed noticeable differences at low frequencies ($f < 1$ MHz), while at high frequencies ($f > 100$ MHz) the levels of dielectric load showed insignificant differences, the values being very close, regardless of the distance between cells or their position.
- Analysis of the electroporation process by numerical modeling of the pore formation dynamics following the application of a train of 50 bipolar pulses and validation of the results obtained with the experimental results from the literature. The 2D numerical model based on axial symmetry developed for this study consists in placing a spherical cell in a cylindrical enclosure and exposing it to different values

of electric field strength, between 0 ... 5000 V/cm, with a step of increment of 1000 V/cm. The calculations were performed for two different extracellular media (low and high values of the electrical conductivity, respectively) taken from the literature. The dynamics of pore formation were calculated and analyzed by integrating the pore density function over time. The obtained results showed that the pore density varies both with the increase of the pause interval between the pulses and with the intensity of the applied electric field. To validate the numerical model, we compared the numerical results with the experimental results from the literature on the percentage of cell permeability, where some quantitative differences were observed due to the elaboration of the numerical model.

List of publications resulting from scientific research in the doctoral program

1. Ana-Maria Sandu, Damijan Miklavčič, Maria Scuderi, Janja Dermol-Černe - "Assessing cancellation effect using numerical modeling of pore formation", Proceedings of "The 30th International Electrotechnical and Computer Science Conference" (ERK), September 2021, pp. 411-414
2. Violeta L. Calin, Mona Mihailescu, Nicolae Tarba, Ana-Maria Sandu, Eugen Scarlat, Mihaela Moisescu and Tudor Savopol - "Digital holographic microscopy evaluation of dynamic cell response to electroporation", Biomedical Optics Express, vol. 12, no. 4, p. 2519, Apr. 2021, doi: 10.1364/BOE.421959, WOS:000636754000004
3. Ana-Maria Sandu, Mihaela Morega - "Electrical stress on membranes in cell suspension, under continuous wave electric field", *12th Int. Symp. Adv. Top. Electr. Eng. ATEE 2021*, Mar. 2021, doi: 10.1109/ATEE52255.2021.9425157, WOS:000676164800061
4. Ana-Maria Sandu, N. Mihale, Mihaela-Andreea Ungureanu, E.I. Scarlat - "Case comparison between direct image compression and hologram compression", U.P.B. Sci. Bull., Series A, Vol. 83, Iss. 1, 2021, WOS:000627614800022
5. Ana-Maria Sandu, Mihaela A. Ungureanu, Mihaela Morega, Violeta L. Călin, Mihaela G. Moisescu, Irina A. Păun, Mona Mihăilescu - "Realistic models of cultured cells for electroporation simulations starting from phase images", Proc. SPIE 11718, Advanced Topics in Optoelectronics, Microelectronics and Nanotechnologies X, Dec. 2020, vol. 11718, p. 37, doi: 10.1117/12.2571092, WOS:000641147900031
6. I.A. Păun, C.C. Mustăciosu, M. Mihăilescu, B.S. Călin, Ana-Maria Sandu - "Magnetically-driven 2D cell organization on superparamagnetic micromagnets fabricated by laser direct writing", Scientific Reports, Vol. 10, no. 1, p. 16418, Dec. 2020, doi: 10.1038/s41598-020-73414-4, WOS:000577151500013
7. Ana-Maria Sandu, Mihaela A. Ungureanu, Mihaela Morega, Violeta L. Călin, Mihaela G. Moisescu, Irina A. Păun, Mona Mihăilescu -"Numerical study on electropermeabilization of cell membranes in sine-wave electric field of variable frequency", *IFMBE Proc.*, vol. 88 Springer Nature Switzerland AG 2022, pp. 365–373, Oct. 2020, doi: 10.1007/978-3-030-93564-1_40.

C3. PERSPECTIVES FOR FURTHER DEVELOPMENT

The directions for further development consist of:

Improving the knowledge of the dynamics of pore formation to follow the variation in time of the electroporation process. To achieve this goal, it is necessary to go through various documentation, testing, and implementing the existing numerical models in this direction.

After understanding how pulsed electric field models work, the next objective is to study the cultivation protocol of adherent cell lines and their use in electroporation experiments, in different working conditions.

Another objective would be to approach other techniques of highlighting the electroporation process, such as transport mechanisms (electrophoresis and diffusion), and to study them both experimentally and numerically.

Another direction to approach is the use of dark-field microscopy images, hyperspectral, and 3D modules , as input models for the realization of numerical models in which different cellular components are highlighted, which can lead to studies of cellular organelles subjected to various parameters related to the electrical properties of the material and the characteristics assigned to the applied electric field.

REFERENCES

[4] M. Morega, *Bioelectromagnetism*. București: Editura Matrix Rom, 1999.

[10] T. Kotnik, L. Rems, M. Tarek, and D. Miklavcic, "Membrane Electroporation and Electropermeabilization: Mechanisms and Models," *Annu. Rev. Biophys.*, vol. 48, pp. 63–91, May 2019, doi: 10.1146/ANNUREV-BIOPHYS-052118-115451.

[22] M. Liberti, F. Apollonio, C. Merla, and G. D'Inzeo, "Microdosimetry in the microwave range: A quantitative assessment at single cell level," *IEEE Antennas Wirel. Propag. Lett.*, vol. 8, pp. 865–868, 2009, doi: 10.1109/LAWP.2009.2028045.

[23] A.-M. Sandu *et al.*, "Realistic models of cultured cells for electroporation simulations starting from phase images," in *Advanced Topics in Optoelectronics, Microelectronics and Nanotechnologies X*, Dec. 2020, vol. 11718, p. 37, doi: 10.1117/12.2571092.

[24] A. M. Sandu *et al.*, "Numerical Study on Electropermeabilization of Cell Membranes in Sine-Wave Electric Field of Variable Frequency," *IFMBE Proc.*, vol. 88, pp. 365–373, Oct. 2020, doi: 10.1007/978-3-030-93564-1_40.

[32] A. Cvetkoska, E. Piro, M. Reberšek, R. Magjarević, and D. Miklavčič, "Towards standardization of electroporation devices and protocols," *IEEE Instrum. Meas. Mag.*, vol. 23, no. 2, pp. 74–81, Apr. 2020, doi: 10.1109/MIM.2020.9062692.

[48] Q. Hu, R. P. Joshi, and D. Miklavcic, "Calculations of Cell Transmembrane Voltage Induced by Time-Varying Magnetic Fields," *IEEE Trans. Plasma Sci.*, vol. 48, no. 4, pp. 1088–1095, Apr. 2020, doi: 10.1109/TPS.2020.2975421.

[49] H. Li *et al.*, "Distributed Effect in High-Frequency Electroporation of Biological Cells," *IEEE Trans. Microw. Theory Tech.*, vol. 65, no. 9, pp. 3503–3511, Sep. 2017, doi: 10.1109/TMTT.2017.2659736.

[54] G. Pucihar, D. Miklavčič, and T. Kotnik, "A time-dependent numerical model of transmembrane voltage inducement and electroporation of irregularly shaped cells," *IEEE Trans. Biomed. Eng.*, vol. 56, no. 5, pp. 1491–1501, May 2009, doi: 10.1109/TBME.2009.2014244.

[58] A. De Angelis *et al.*, "A Microdosimetric Realistic Model to Study Frequency-Dependent Electroporation in a Cell with Endoplasmic Reticulum," in *2019 49th European Microwave Conference, EuMC 2019*, Oct. 2019, pp. 212–215, doi: 10.23919/EuMC.2019.8910909.

[86] V. L. Calin *et al.*, "Digital holographic microscopy evaluation of dynamic cell response to electroporation," *Biomed. Opt. Express*, vol. 12, no. 4, p. 2519, Apr. 2021, doi: 10.1364/BOE.421959.

[88] I. A. Paun, C. C. Mustaciosu, M. Mihailescu, B. S. Calin, and A. M. Sandu, "Magnetically-driven 2D cells organization on superparamagnetic micromagnets fabricated by laser direct writing," *Sci. Rep.*, vol. 10, no. 1, p. 16418, Dec. 2020, doi: 10.1038/s41598-020-73414-4.

[97] H. Schwan, "Electrical properties of tissue and cell suspensions," *Adv. Biol. Med. Phys.*, vol. 5, pp. 147–209, 1957, doi: 10.1016/B978-1-4832-3111-2.50008-0.

[99] C. Polk and E. Postow, *CRC Handbook of Biological Effects of Electromagnetic Fields*. CRC Press, Taylor & Francis Group, 1986.

[100] T. Kotnik and D. Miklavčič, "Analytical Description of Transmembrane Voltage Induced by Electric Fields on Spheroidal Cells," *Biophys. J.*, vol. 79, no. 2, pp. 670–679, Aug. 2000, doi: 10.1016/S0006-3495(00)76325-9.

[101] C. Merla, M. Liberti, F. Apollonio, and G. D'inzeo, "Quantitative assessment of dielectric parameters for membrane lipid bi-layers from RF permittivity measurements," *Bioelectromagnetics*, vol. 30, no. 4, pp. 286–298, May 2009, doi: 10.1002/BEM.20476.

[112] A. M. Sandu and M. Morega, "Electrical Stress on Membrane for Cells in Suspension under Continuous Wave Electric Field," 12th Int. Symp. Adv. Top. Electr. Eng. ATEE 2021, Mar. 2021, doi: 10.1109/ATEE52255.2021.9425157.

[113] T. Polajžer, J. Dermol-Černe, M. Reberšek, R. O'Connor, and D. Miklavčič, "Cancellation effect is present in high-frequency reversible and irreversible electroporation," *Bioelectrochemistry*, vol. 132, Apr. 2020, doi: 10.1016/J.BIOELECHEM.2019.107442.

[115] M. Scuderi, M. Rebersek, D. Miklavcic, and J. Dermol-Cerne, "The Use of High-frequency Short Bipolar Pulses in Cisplatin Electrochemotherapy in Vitro," *Radiol. Oncol.*, vol. 53, no. 2, p. 194, 2019, doi: 10.2478/RAON-2019-0025.

[123] L. Rems, M. Ušaj, M. Kandušer, M. Reberšek, D. Miklavčič, and G. Pucihar, "Cell electrofusion using nanosecond electric pulses," *Sci. Reports 2013 31*, vol. 3, no. 1, pp. 1–10, Nov. 2013, doi: 10.1038/srep03382.

[125] A.-M. Sandu, D. Miklavčič, M. Scuderi, and J. Dermol-Černe, "Assessing cancellation effect using numerical modeling of pore formation," in *ERK*, 2021, pp. 411–414.